TYPE Original Research
PUBLISHED 05 September 2022
DOI 10.3389/feart.2022.982037

OPEN ACCESS

EDITED BY
Shengyao Yu,
Ocean University of China, China

REVIEWED BY
Hao Cheng,
Tongji University, China
Zaibo Sun,
Yunnan Institute of Ggieolocal Survey,
China

*CORRESPONDENCE
Zhimin Peng,
pzm20022002@163.com

SPECIALTY SECTION
This article was submitted to Petrology,
a section of the journal
Frontiers in Earth Science

RECEIVED 30 June 2022
ACCEPTED 27 July 2022
PUBLISHED 05 September 2022

CITATION
Fu Y, Peng Z, Wang G, Hu J, Zhang Z, Guan J and Ren F (2022), Paleo-Tethys subduction and arc-continent collision: Evidence from zircon U-Pb chronology, geochemistry and Sr-Nd-Hf isotopes of eclogites in western Yunnan, bangbing area, southeastern Tibetan Plateau.
Front. Earth Sci. 10:982037.
doi: 10.3389/feart.2022.982037

Paleo-Tethys subduction and arc-continent collision: Evidence from zircon U-Pb chronology, geochemistry and Sr-Nd-Hf isotopes of eclogites in western Yunnan, bangbing area, southeastern Tibetan Plateau

Yuzhen Fu[1,2], Zhimin Peng[1,3]*, Guozhi Wang[1,2], Jingfeng Hu[4], Zhang Zhang[3], Junlei Guan[3] and Fei Ren[3]

[1]College of Earth Sciences, Chengdu University of Technology, Chengdu, China, [2]Key Laboratory of Tectonic Controls on Mineralization and Hydrocarbon Accumulation of Ministry of Natural Resources, Chengdu University of Technology, Chengdu, China, [3]Chengdu Center of China Geological Survey, Chengdu, China, [4]Institute No 280 of CNNC, Guanghan, China

The Changning-Menglian suture zone (CMSZ) in the southeastern Tibetan Plateau is a newly discovered HP-UHP metamorphic zone. The eclogites therein are the key evidence constraining the main suture of the Proto- and Paleo-Tethys Ocean in western Yunnan. Targeting the weakly studied Bangbing eclogites, we developed a comprehensive study on the whole-rock compositions, Sr-Nd isotope and zircon U-Pb ages, zircon trace elements and Lu-Hf isotope to reveal the subduction and arc-land collision. The eclogites occur as massive blocks or lenses and embedded in garnet phengite quartz schists of Lancang Group, Early Paleozoic accretionary complex. Their geochemistry is similar to E-MORB, and exhibit isotopic $\varepsilon_{Nd}(t)$ values of 3.14–4.49 and $\varepsilon_{Hf}(t)$ of 14.64–16.41, respectively. The Nb-enriched mafic protoliths suggested they were probably generated by partial melting of the enriched oceanic mantle within the spinel stability field and emplaced or erupted as mid-ocean ridge in the Paleo-Tethys Ocean. By LA-ICP-MS zircon U-Pb age testing, the magmatic zircon grains separated from the eclogites yield a wide range of ages, which may be capture zircon ages rather than protolith crystallization. We infer the age of eclogite-facies metamorphism to be 238 ± 2 Ma based on CL images, zircon trace element analysis, and that this metamorphism marks the collision between the Eastern Lincang magmatic arc, the Simao block and the Western Baoshan block. Thus, exhumation of the eclogites occurred only 7 to 23 Ma later, according to age 231–215 Ma for post-collisional volcanic and granitic rocks east of the CMSZ. Conclusively, the continued subduction of the Paleo-Tethys oceanic crust occurred during the Early-Middle Triassic, and rapid exhumation in the Late Triassic. The Changning-Menglian suture zone is a typical oceanic subduction-accretionary orogeny belt.

KEYWORDS

eclogite, zircon U-Pb, Sr-Nd-Hf isotope, Paleo-Tethys, Changning-Meglian suture zone

Introduction

The Changning-Menglian suture zone (CMSZ) locates in the southeastern Tibetan Plateau and represents the eastern part of the global Tethys tectonic domain. As an important "window" for investigating the evolution of Proto- and Paleo-Tethys in the Sanjiang region, it has been attracting great attention from geologists. Recently, it has been increasingly recognised that this suture zone shared similar geological evolution with the Longmucuo-Shuanghu suture zone (LSSZ) in the central Tibetan Plateau (Pan et al., 1997; Zhong 1998; Metcalfe, 2013; Deng et al., 2014). The two together represent the remains of the eventual disappearance of the Proto- and Paleo-Tethys Ocean, and record the magnificent geological history of subduction and arc-continent collisional orogenesis (Pan et al., 2004; Wang D.B. et al., 2016; Wang B.D. et al., 2013, 2018; Peng et al., 2020a). Understanding the evolutionary history of the Eastern Paleo-Tethys is essential for reconstructing the Asian tectonics and geodynamics.

As significant signatures of convergent slab boundary, high-pressure/ultra-high-pressure (HP/UHP) metamorphic rocks (e.g., eclogite, blueschist) record the dynamics of subduction and exhumation in oceanic and/or continental crust (Maruyama et al., 1996; Ernst, 2006; Zhang et al., 2008; Wei and Clarke, 2011). A number of typical eclogites and blueschists related to the evolution of the oceanic crust have been identified in the LSSZ, and rich research results have been published (e.g., Bao et al., 1999; Li et al., 2006, 2008, 2009; Dong and Li, 2009, 2010; Zhai et al., 2009, 2011, 2017; Zhang et al., 2010, 2014; Liu et al., 2011; Liang et al., 2017). In contrast, previous studies in the CMSZ have focused on the blueschists discovered in the Lancang Group in the early 1980s, concentrating on their spatial distribution, chronology, petrography and P-T conditions (e.g., Peng and Luo, 1982; Zhang et al., 1990; Zhao, 1993, 1994; Zhang et al., 2004; Fan et al., 2015; Wang DB. et al., 2016). Subsequently, Li Jing et al. (2015; 2017) first identified garnet-amphibolites in the Wanhe ophiolite mélange, and further studies by Wang et al. (2019) suggest that those rocks should be lawsonite-bearing retrograded eclogites. Recently, with the 1:50,000 regional geological survey in western Yunnan, a large number of eclogites and blueschists have been continuously identified along Changning, Shuangjiang and Lancang areas (Peng et al., 2019; Sun et al., 2019; Wang et al., 2020a, 2020b; Fu et al., 2021). These HP/UHP metamorphic rocks extend intermittently for about 600 km, structuring a giant HP/UHP metamorphic belt (Figure 1A). It makes the CMSZ a hotspot for the tectonic evolution studies of Paleo-Tethys.

In the CMSZ, the eclogites are mainly outcropped from north to south in the Mengku, Bangbing, Qianmai and Jinghong areas. Currently, some research has been conducted on the petrogenesis, chronology and P-T metamorphic evolution of the eclogites rocks from Mengku, Qianmai and Jinghong areas (Sun et al., 2019; Wang et al., 2020b; Zhao et al., 2021). Meanwhile, studies on the petrology and metamorphism of the eclogites in Bangbing area have been limited (Peng et al., 2019, 2020b; Fu et al., 2021). For this area, we are still not clear about such questions as the origin of the protoliths, the ages of the protoliths and metamorphism, and whether these features correspond to the evolution of regional metamorphic zones. Therefore, in this paper, further chronological, geochemical studies and isotopic analyses of the Bangbing eclogites are presented to investigate the evolution and accretionary orogeny of the Tethys Ocean in western Yunnan.

Geological background and samples

Geological background

The Changning-Menglian suture zone is located in southeastern Tibetan Plateau, and extends north-south for 600km, bordering the Lingcang-Menghai magmatic arc to the east, separating the Baoshan Block to the west from the Simao Block to the east (Figure 1B; Metcalfe, 2013; Wang et al., 2018). The study area falls along the Bangbing area of Shuangjiang County in the suture zone. The area is characterised by the Early Paleozoic-Late Triassic oceanic crust formations. The formations are mainly composed of Early Ordovician-Middle Triassic Niujinshan ophiolitic mélange, Carboniferous-Permian oceanic island-seamount strata, i.e., oceanic island basalt and its siliciclastic and carbonate cover, Devonian -Permian deep-sea or bathyal silica-mud assemblages, and Early Paleozoic accretionary complex (Wang et al., 2018; Peng et al., 2020b). The Upper Triassic Sanjiahe Group (T_3sc) and the Middle Jurassic Huakaizuo Group (J_2h), which are continental sedimentary clastic rocks, unconformably overlie these different oceanic formations, with the T_3sc representing the earliest sedimentary cover after the disappearance of the Changning-Menglian Ocean (Wang et al., 2018).

The widely outcropped accretionary complex in the CMSZ is mainly composed of the Lancang Group. The rocks are complex in composition and can be divided into "matrix" and "block" (Peng et al., 2020b). The matrix is mainly metasedimentary rocks, represented by mica quartz schist, garnet mica schist and carbonaceous mica schist. The blocks are composed of various rocks, including metavolcanic rocks (greenschist, albite schist, amphibole schist, etc.), metamorphic intermediate acid intrusive

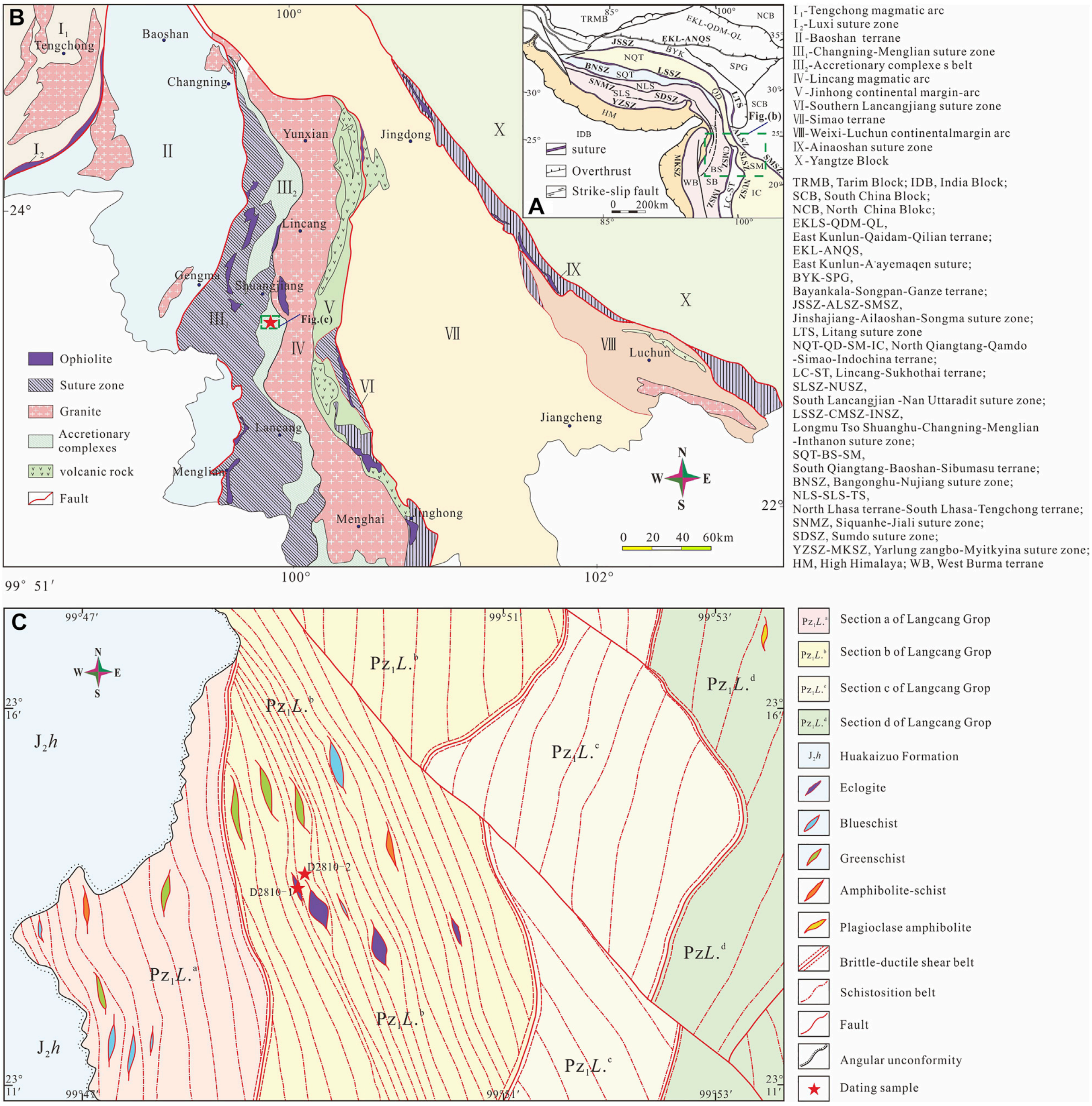

FIGURE 1
Tectonic framework of the East Tethys tectonic domain (**A**, after Xu et al., 2015), geotectonic view of the Changning-menglian orogenic system **(B)** and geological sketch of the Bangbing area **(C)**. (Fig.a after Xu et al., 2020).

rocks (granitic gneisses, albite leptynite) and HP metamorphic rocks (blueschist, eclogites, etc.). Based on whole-rock Rb-Sr and Sm-Nd isotope data and the fossil records, the Lancang Group was previously considered to be the Precambrian basement (Zhai et al., 1990; Zhong, 1998). However, zircon U-Pb age data from the metavolcanic and metaclastic rocks (462–454 Ma, 450–428 Ma, respectively) suggest that the depositional age was Late Ordovician-Silurian rather than Neoproterozoic (Nie et al., 2015; Xing et al., 2017; Wang F. et al., 2017; Wang B.D. et al., 2018). The Lancang Group is divided into several formations and rock sections (Figure 1C), all of which are in tectonic contact with each other, and the original stratigraphy has been completely replaced and the original sedimentary structure has been destroyed (Peng et al., 2020b).

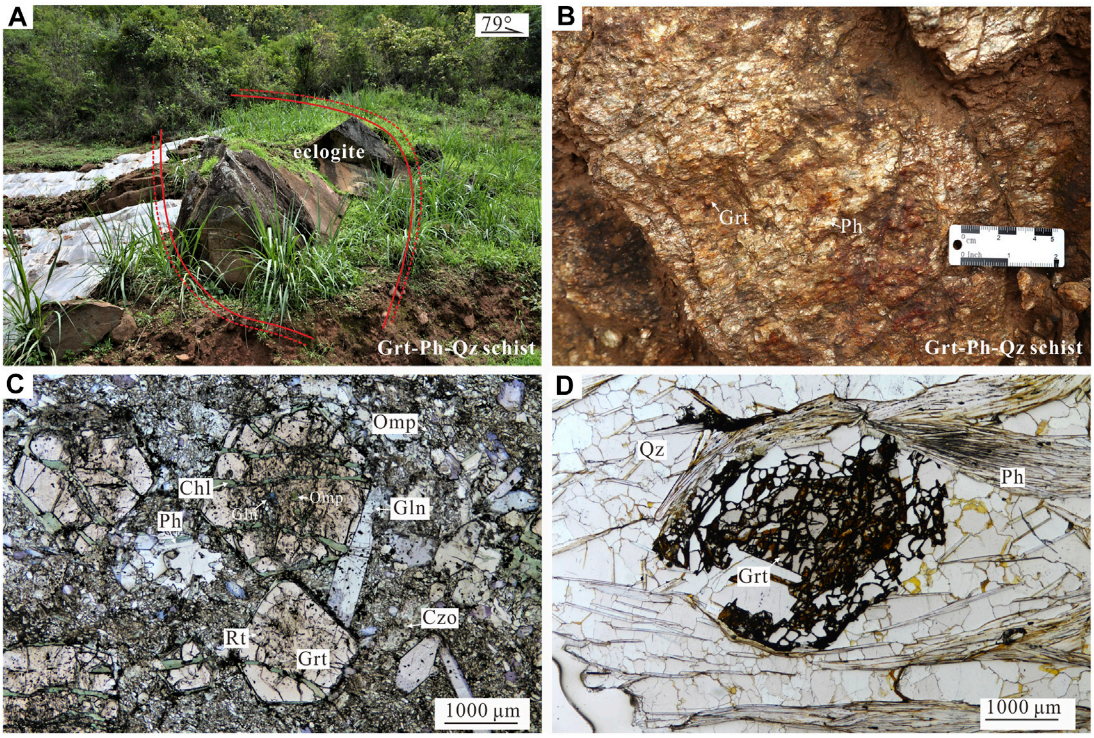

FIGURE 2
Field characteristics and microphotographs of the eclogites and their surrounding schists in Bangbing area. **(A)**, The eclogites (sample D2810-1) are lens-shaped, with strong foliations at the contact boundary to the surrounding rocks. **(B)**, The eclogites are surrounded by coarse-grained garnet phengite schists (sample D2810-2). **(C)**, The eclogite mainly consists of garnet, omphacite and glaucophane, with minor phengite, quartz, clinozoisite and rutile. **(D)**, Grt-Ph-Qz schist show well-developed foliation, and defined by fine layers of phengite, with garnet enclosed by the layers.

Samples description

The eclogites occur as massive blocks or lenses and embedded in schist (Figure 2A). The eclogites appear as tectonic sheets and the contact boundary with the schist is strongly foliated. The field characteristics and petrographic studies of Bangbing eclogite and its enclosing rocks have been discussed in detail previously (Peng et al., 2019; Fu et al., 2021). The Bangbing eclogite mainly consists of garnet, omphacite and glaucophane, with minor phengite, quartz, clinozoisite and rutile (Figure 2C). The clinozoisite is likely to have been transformed from lawsonite by dehydration (Clarke et al., 2006; Wei and Clarke, 2011). Several HP metamorphic rock samples in the CMSZ have identified lawsonite inclusions preserved in garnet or glaucophane (Wang et al., 2019; 2020a). The coexistence of lawsonite and glaucophane in the eclogite strongly points to a cold oceanic crust subduction. The peak P-T conditions of Bangbing eclogites were estimated at 3.0–3.2 GPa and 617–658°C by the Grt-Omp-Phn geothermobarometer (Fu et al., 2021). Correspondingly, researchers combined with phase equilibrium simulations to obtain peak P-T conditions for HP rocks in different locations in the CMSZ, such as 2.4–2.6 GPa, 520–530°C for lawsonite-bearing retrograded eclogite in the Mengku area (Wang et al., 2019); 2.3–2.6 GPa, 570–610°C for phengite/talc-glaucophane eclogites in the Heihe area; and 2.9 GPa, 600°C for glaucophane eclogites, 2.85–2.96 GPa, 580–594°C for dolomite–kyanite eclogites, and 675–754°C, 2.9–3.2 GPa for magnesite–kyanite eclogites, respectively, in the Qianmai area (Sun et al., 2019; Wang et al., 2020b; Wang W. et al., 2021).

The garnet phengite quartz (Grt-Ph-Qz) schists are the direct country rocks of the Bangbing eclogite body (Figure 2B). Grt-Ph-Qz schists are coarse grained and consist mainly of quartz (50%), phengite (35%), garnet (10%) and minor accessory mineral (5%) such as apatite and sphene. Quartz schists show well-developed foliation, and defined by fine layers of phengite, with garnet enclosed by the layers (Figure 2D). The mineral assemblages and microstructure suggest that quartz schists have suffered high pressure metamorphism. The peak P-T conditions of 1.88–2.16 GPa and 392–553°C were obtained by previous phase equilibrium simulations. The metamorphic zircon U-Pb and phengite $^{40}Ar/^{39}Ar$ isotopic analyses in the schist yielded consistent peak HP ages of 238–235 and 237–231 Ma, respectivel. A significant volume of sediments from the Lancang Group may have been subducted to a depth of ~60–80 km in the Middle Triassic during the closure of the Paleotesti Ocean (Wang et al., 2020a).

The eclogite samples investigated in this work were collected from the Bangbin area, about 150 km south of Lincang (Figure 1B). The fresh eclogite samples (Sample D2810-1) from section b of the Lancang Group (Figure 1C) were selected for whole-rock major and trace element, and whole-rock Sr-Nd isotope analyses. The zircons separated from them were measured for U-Pb dating, trace element and Lu-Hf isotopic analyses. Comparatively, zircons separated from one surrounding rock sample (Sample D2810-2), a Grt-Ph-Qz schist, were also analysed for U-Pb dating. The two sampling sites were less than 50 m apart. Mineral abbreviations in this study are after Whitney and Evans (2010).

Analytical methods

Whole-rock major and trace elements

Major and trace element analyses of whole-rock geochemistry were conducted on X-ray fluorescence spectrometry (XRF, Primus II, Rigaku, Japan), inductively coupled plasma-mass spectrometry (ICP-MS, Agilent, 7,700 e, United States) at the Wuhan Sample Solution Analytical Technology Company Co., Ltd. Before analyses, samples were crushed and powdered to 200-mesh in an agate mill; then the sample powders were dried at 105°C in an oven. Four standards (AGV-2, BHVO-2, BCR-2 and RGM-2) were used to monitor the analytical quality. The relative standard deviations for the trace elements are within ±5%.

Zircon U-Pb dating, trace element and Lu-Hf isotopic

Zircons were separated by conventional heavy liquid and magnetic techniques at the Langfang Chengxin Geological Service Company (Hebei, China). Then they were handpicked under a binocular microscope, mounted in epoxy and polished to about half section. Cathodoluminescence (CL) images of zircon grains were taken on a Gatan Mono CL4 Cathode-Luminescence detector attached to a Zeiss Sigma 300 field emission SEM at the Wuhan Sample Solution Analytical Technology Company Co., Ltd., to observe the internal structure and to target potential sites for zircon U-Pb-Hf isotopic analyses.

In situ zircon U-Pb dating and trace element compositions were simultaneously analyzed by LA-ICP-MS at the Wuhan SampleSolution Analytical Technology Co., Ltd. China. Detailed operating conditions for the laser ablation system and the ICP-MS instrument and data reduction are the same as those described by Liu YS. et al. (2008). Laser sampling was performed using a GeolasPro laser ablation system that consists of a COMPexPro 102 ArF excimer laser (wavelength of 193 nm and maximum energy of 200 mJ) and a MicroLas optical system. An Agilent 7,700 e ICP-MS instrument was applied to acquire ion-signal intensities. Helium was applied as a carrier gas, which is mixed with Argon, the make-up gas, *via* a T-connector before entering the ICP. In this study, the spot size and frequency of the laser were set to 32 μm and 5 Hz, respectively. For every five analyses, zircon 91500, GJ-1 and glass NIST610 were used as external standards for U-Pb dating and trace element calibration. Each analysis incorporated a background acquisition of ~20–30 s followed by 50 s of data acquisition from the sample. Raw data were processed using an Excel-based software ICPMSDataCal (Liu et al., 2010). Concordia diagrams and age calculations were made using the program Isoplot/Ex_ver3 (Ludwig, 2003).

In situ zircon Lu-Hf isotopic analysis was conducted using a Neptune Plus MC-ICP-MS (Thermo Fisher Scientific, Germany) in combination with a Geolas HD excimer ArF laser ablation system (Coherent, Göttingen, Germany) at the Wuhan Sample Solution Analytical Technology Co., Ltd. China. In this study, all data were acquired on zircon in single spot ablation mode at a spot size of 44 μm, and the energy density of laser ablation was ~7.0 J cm^{-2}. Each measurement consisted of 20 s of acquisition of the background signal followed by 50 s of ablation signal acquisition. Detailed operating conditions for the laser ablation system and the MC-ICP-MS instrument and analytical method can be found in Hu et al. (2012). The calculated parameters used in this study are ^{176}Lu decay constants of 1.867×10^{-11} a^{-1} (Söderlund et al., 2004), ^{176}Hf/^{177}Hf and ^{176}Lu/^{177}Hf ratios of 0.2827720 and 0.0332 for Spherulitic meteorites, respectively (Blichert-Toft and Albarede., 1997), and present deficit mantle values of ^{176}Hf/^{177}Hf = 0.28325 and ^{176}Lu/^{177}Hf = 0.0384 (Griffin et al., 2000).

Whole-rock Sr-Nd isotopic

Whole-rock Sr-Nd-Pb isotopic analyses were carried out on a Neptune Plus MC-ICP-MS (Thermo Fisher Scientific, Dreieich, Germany) at the Wuhan Sample Solution Analytical Technology Co., Ltd., China. All chemical preparations were made on class 100 work benches within a class 1,000 over-pressured clean laboratory. The detailed methods and instrumentation for Sr-Nd isotopic analyses have been described by Li et al. (2012). During the Sr-Nd isotopic analyses, the NIST SRM 987 standard solution yielded ^{87}Sr/^{86}Sr ratio of 0.710,244 ± 0.000022 (2SD, n = 32) and the JNdi-1 106 standard gave ^{143}Nd/^{144}Nd ratio of 0.512118 ± 0.000015 (2SD, n = 31). In addition, the USGS107 reference materials BCR-2 (basalt) and RGM-2 (rhyolite) yielded results of 0.705034 ± 0.000014 (2SD, n = 4) and 0.704192 ± 0.000010 (2SD, n = 4) for ^{87}Sr/^{86}Sr, 0.512644 ± 0.000015 (2SD, n= 6) and 0.512810 ± 0.000015 (2SD, n = 4) for ^{143}Nd/^{144}Nd, respectively, both of which are identical within error to their published values (Li et al., 2012).

TABLE 1 Major, trace elements and Sr-Nd isotopes for the Bangbing eclogites.

Sample	D2810-1H1	D2810-1H2	D2810-1H3	D2810-1H4	D2810-1H5	D2810-1H6	D2810-1H7
Major element (%)							
SiO_2	47.77	46.49	47.00	45.92	47.02	50.95	49.65
TiO_2	2.01	2.00	1.98	2.01	2.07	1.44	1.46
Al_2O_3	14.74	14.58	14.53	14.78	15.00	15.23	15.60
TFeO	14.03	14.36	14.63	14.95	14.41	9.26	9.97
MnO	0.19	0.26	0.25	0.27	0.21	0.18	0.18
MgO	5.25	5.45	5.87	5.97	5.52	6.50	6.76
CaO	12.01	12.14	11.35	11.71	11.78	11.74	11.45
Na_2O	2.67	2.49	2.88	2.61	2.64	2.81	2.60
K_2O	0.16	0.24	0.39	0.32	0.39	0.18	0.49
P_2O_5	0.22	0.25	0.24	0.22	0.22	0.15	0.16
LOI	0.39	1.06	0.01	0.51	0.10	0.93	1.33
Trace element (ppm)							
Sc	37.66	37.68	37.10	38.44	39.59	36.17	37.24
V	305.27	310.12	301.04	307.49	311.88	317.23	319.78
Cr	148.33	156.04	155.58	163.34	144.29	123.51	130.67
Co	39.11	42.22	42.24	43.22	42.93	38.88	43.28
Ni	58.76	62.62	62.87	63.88	60.72	61.86	66.28
Cu	48.47	48.61	48.90	55.64	50.04	68.95	75.61
Zn	106.03	109.10	109.41	112.39	113.88	81.96	88.89
Ga	20.00	20.13	19.37	19.34	20.17	18.93	19.50
Rb	4.28	6.47	8.23	8.06	8.25	3.98	12.01
Sr	196.30	184.27	131.38	145.64	198.45	104.02	124.07
Y	50.28	47.38	49.32	50.80	52.05	27.46	27.52
Zr	175.28	175.65	164.53	170.40	177.46	97.19	98.34
Nb	14.35	14.55	14.62	15.26	15.68	9.02	9.23
Cs	0.88	1.38	0.94	1.40	0.77	0.37	1.19
Ba	19.73	29.75	51.38	40.73	50.93	21.32	50.06
La	14.03	14.08	13.01	12.75	15.91	9.56	8.01
Ce	31.02	31.80	29.43	29.45	34.78	21.54	19.72
Pr	4.18	4.20	3.95	4.04	4.66	2.87	2.80
Nd	19.22	19.15	17.92	18.12	21.52	13.51	13.17
Sm	5.23	5.37	5.15	5.28	6.01	3.93	3.90
Eu	1.76	1.66	1.63	1.70	1.86	1.32	1.30
Gd	6.77	6.73	6.77	6.66	7.24	4.89	4.65
Tb	1.25	1.20	1.26	1.24	1.28	0.78	0.75
Dy	8.03	7.75	8.28	8.45	8.44	4.73	4.67
Ho	1.72	1.76	1.77	1.83	1.84	0.94	0.99
Er	4.62	4.39	4.46	4.72	4.80	2.66	2.73
Tm	0.71	0.69	0.69	0.73	0.74	0.38	0.38
Yb	4.94	4.84	4.87	5.05	5.21	2.54	2.35
Lu	0.68	0.66	0.65	0.73	0.72	0.40	0.39
Hf	4.69	4.74	4.56	4.65	4.79	2.50	2.66
Ta	0.97	1.01	0.99	1.02	1.02	0.53	0.54
Pb	1.46	1.31	0.98	1.12	2.97	6.87	4.24
Th	1.69	1.69	1.67	1.57	1.80	1.05	1.08
U	0.53	0.51	0.43	0.48	0.97	0.28	0.24
∑REE	104	104	100	101	115	70	66

(Continued on following page)

10.3389/feart.2022.982037

TABLE 1 (*Continued*) Major, trace elements and Sr-Nd isotopes for the Bangbing eclogites.

Sample	D2810-1H1	D2810-1H2	D2810-1H3	D2810-1H4	D2810-1H5	D2810-1H6	D2810-1H7
δEu	0.90	0.84	0.85	0.88	0.86	0.92	0.93
$(La/Yb)_N$	2.04	2.08	1.92	1.81	2.19	2.70	2.45
$(La/Sm)_N$	1.73	1.69	1.63	1.56	1.71	1.57	1.32
Sr-Nd-Pb isotopes							
$^{87}Sr/^{86}Sr$	0.705,797	0.711922	0.707300			0.712837	0.708815
$^{143}Nd/^{144}Nd$	0.512773	0.512764	0.512731			0.512746	0.512750
$(^{87}Sr/^{86}Sr)t$	0.705392	0.711269	0.706136			0.712126	0.707016
$(^{143}Nd/^{144}Nd)t$	0.512287	0.512263	0.512218			0.512227	0.512221
εNd(t)	4.49	4.02	3.14			3.32	3.20

$(^{143}Nd/^{144}Nd)_t$ $(^{206}Pb/^{204}Pb)_t$, $\varepsilon_{Nd}(t)$ Values are calculated from t = 451 Ma. Parameters used for samples calibration $(^{143}Nd/^{144}Nd)_t=(^{143}Nd/^{144}Nd)_{sample}(^{147}Sm/^{144}Nd)_m\times(e^{\lambda t}-1)$, $\varepsilon_{Nd}(t)=[(^{143}Nd/^{144}Nd)_t/(^{143}Nd/^{144}Nd)_{CHUR(t)}-1]\times10^4$ $(^{143}Nd/^{144}Nd)_{CHUR(t)}=0.512,638-0.1967\times(e^{\lambda t}-1)$, $\lambda_{Sm-Nd}=6.54\times10^{-12}a^{-1}$.

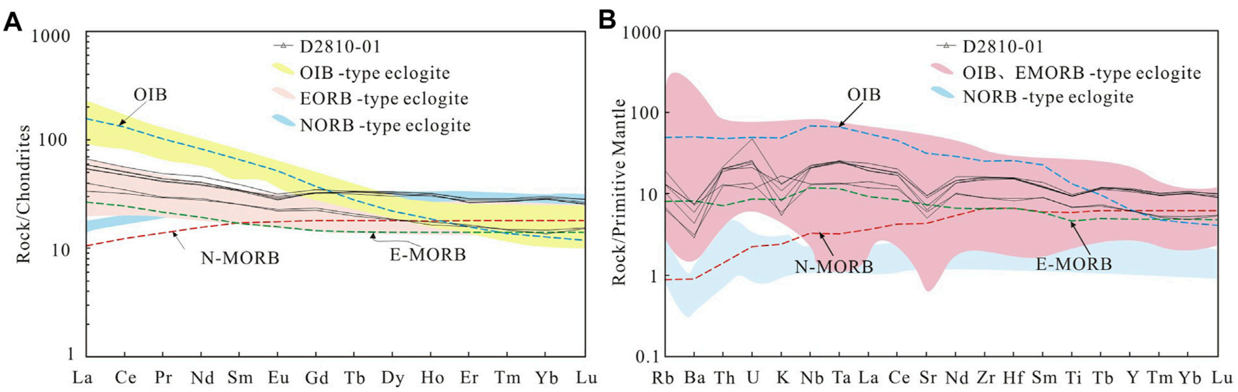

FIGURE 3
Chondrite-normalized rare earth element patterns **(A)** and primitive mantle-normalized trace element patterns **(B)** for Bangbing eclogites.

Results

Whole-rock major and trace elements

The major and trace elements in the Bangbing eclogites are listed in Table 1. The eclogites show losses of volatiles on ignition (LOI) ranging from 0.01 to 1.33 wt% with an average value of 0.62 wt%, indicating variable alteration of the rocks. All the eclogites samples have SiO_2 contents ranging from 45.92 to 50.59 wt%, averaging 47.83 wt%, with characteristics of basaltic. These samples are characterized by low MgO (5.25–6.76 wt%) contents, relatively high Al_2O_3 (14.53–15.60 wt%) and CaO (11.35–112.14 wt%) contents. K_2O/Na_2O ratios of 0.06–0.19 <1 and low all-alkaline (Na_2O+K_2O) contents (2.82–3.09 wt%) in the eclogites show compositional features corresponding to tholeiite basalt.

The total rare earth contents (∑REE) in the samples ranged from 66.00 to 115 ppm with an average of 94 ppm, which is higher than the typical E-MORB total REE (49.09×10^{-6}) and lower than the OIB total REE (Sun and McDonough, 1989). The chondrite normalized REE diagrams show that all the eclogites samples exhibit REE patterns characterized by light REE (LREE) enrichment, heavy REE (HREE) depletion and low degrees of LREE and HREE fractionation ($(La/Yb)_N$=1.81–2.70, averaging 2.17 $(La/Sm)_N$ = 1.32–1.73, averaging 1.60), and no significant negative Eu anomalies (δEu=0.84–0.93, averaging 0.88) (Figure 3A).

Normalized to primitive mantle, all the eclogites are characterized by a wide range of large ion lithophile elements (LILEs, e.g., Rb, Ba, K, U and Sr), a narrow range of high field-strength elements (HFSEs, e.g., Nb, Ta, Zr and Hf). The Ti in the samples has a slight negative anomaly, possibly affected by subduction fluids (Zheng, 2012). The trace elements are not

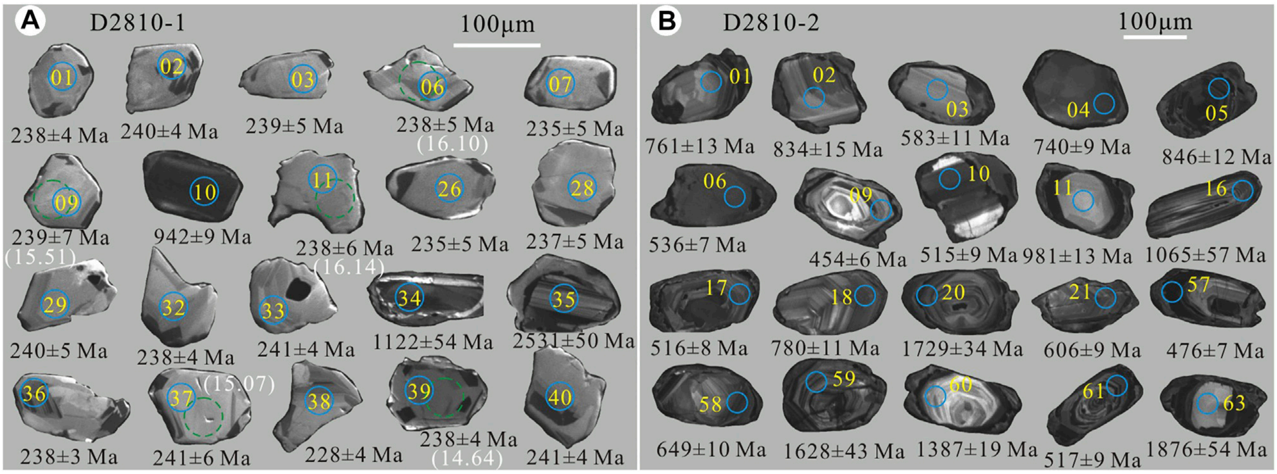

FIGURE 4
Zircon cathodoluminescence images and U-Pb ages, Hf isotope test spots for eclogites **(A)** and Grt-Ph schists **(B)**. Blue circles represent zircon analysis spots and green circles represent Hf isotope analysis spots. Data greater than 1,000 Ma follow ^{207}Pb/^{206}U ages, the rest follow ^{206}Pb/^{238}U ages.

obviously depleted or enriched and show nearly flat distribution patterns. These characteristics fall between E-MORB and OIB, and tend to be more in line with the former (Figure 3B).

Zircon U-Pb geochronology

Zircon grains were analysed from eclogite D2810-1 and its surrounding Grt-Ph-Qz schist D2810-2, separately. The CL images are presented in Figure 4. The U–Pb age data are listed in Table 2 and present in Figure 4.

In sample D2810-1, zircon grains are subhedral to euhedral crystal of plate. The lengths range from 60 to 150 μm with the aspect ratios of 1:1 to 1.5:1. (Figure 4). Some of them exhibit clear core–rim structures in cathodoluminescence (CL) images. The cores are zoned with dark or light grey oscillatory bands. The other part of the zircons show no core–rim structure or oscillating bands. The grains are more homogeneous internally and surrounded by narrow and bright overgrowths, indicative of a metamorphic origin. Forty spot analyses show ^{206}Pb/^{238}U ages ranging from 220 to 2,470 Ma and can be divided into three groups. Group I, ^{206}Pb/^{238}U ages, vary over a wide range from 256 to 2,470 Ma. The zircons obtained from this data group majority have core-rim structures with wide ranges of variation in Th and U content and high Th/U ratios (Th/U=0.12–6.91, Figure 5B), indicating magmatic zircon characteristics and may be captured. The second and third data groups are from zircons that show no rims, no cores and no oscillating rings. Group II ^{206}Pb/^{238}U ages range from 235 to 241 Ma, with U and Th contents of 43×10^{-6}–304 and 0.15–2.83 ppm, having low Th/U ratios of 0.004–0.01, much less than 0.1 (Figure 5B), indicative of a metamorphic origin. All twenty-five data spots in this group cluster on or near the harmonic line (Figure 5A), with a weighted mean of 238 ± 2 Ma (MSWD = 1.6). Discussion of this group of age data will be continued later. Group III of age data contains three spots. The zircon ^{206}Pb/^{238}U ages range from 220 to 229 Ma and, similar to the second group, have low Th/U ratios of 0.004–0.009, much less than 0.1 (Figure 5B), likely to represent much later ages of metamorphism.

In sample D2810-2, the morphology of the zircon grains appears to be more various than in the eclogites. The zircon grains are in long and short columns, 100–200 μm long. In the CL images, some grains show clear core-rim structure with an irregular, weakly luminescent, broad band in the core; some grains show homogeneous, undivided structure; while the other grains have distinct oscillatory bands of magmatic origin (Figure 4B). A total of 89 analyses on these zircons show high Th/U ratios ranging from 0.06 to 1.63 (only 4 spots less than 0.1), which generally correspond to the ranges of Th/U ratios of Group I capture- origin zircons from sample D2810-1 (Figure 5B). The ages range from 454 to 3,591 Ma (>1,000 Ma follow the ^{207}Pb/^{206}U age, the rest follow the ^{206}Pb/^{238}U age), and they have excellent harmonics (all >90% and most above 95%), all falling on or near the harmonic line (Figure 5C). In the zircon U-Pb age frequency histograms there are three dominant groups of age peaks, the youngest of which is around 450–600 Ma, with the rest at 700–1,200 Ma and 1,250–1800 Ma (Figure 5D).

Zircon trace elements

The zircon trace element content of the eclogite (sample D2810-1) is shown in Table 3. In the chondrite normalized REE

TABLE 2 Zircon LA-ICP-MS U-Pb age analysis results for Bangbing eclogites and their surrounding Grt-Ph schists.

Sample spot	Content ($\times10^{-6}$)		Th/U	Isotope ratio						Age/Ma					
	Th	U		$^{207}Pb/^{206}Pb$	1sigma	$^{207}Pb/^{235}U$	1sigma	$^{206}Pb/^{238}U$	1sigma	$^{207}Pb/^{206}Pb$	1sigma	$^{207}Pb/^{235}U$	1sigma	$^{206}Pb/^{238}U$	1sigma
D2810-1 Eclogites															
D2810-1-01	0.82	162	0.005	0.0551	0.0045	0.2779	0.0194	0.0377	0.0007	417	179	249	15	238	4
D2810-1-02	2.05	206	0.010	0.0506	0.0029	0.2654	0.0150	0.0380	0.0006	220	131	239	12	240	4
D2810-1-03	0.46	110	0.004	0.0563	0.0048	0.2826	0.0205	0.0377	0.0008	465	191	253	16	239	5
D2810-1-04	2.83	304	0.009	0.0524	0.0028	0.2692	0.0133	0.0371	0.0005	306	122	242	11	235	3
D2810-1-05	158	240	0.659	0.0527	0.0024	0.5426	0.0238	0.0744	0.0010	317	104	440	16	463	6
D2810-1-06	0.65	127	0.005	0.0531	0.0044	0.2736	0.0209	0.0375	0.0008	332	155	246	17	238	5
D2810-1-07	0.34	70	0.005	0.0532	0.0060	0.2606	0.0252	0.0371	0.0008	339	257	235	20	235	5
D2810-1-08	2.44	260	0.009	0.0498	0.0028	0.2415	0.0126	0.0348	0.0006	187	130	220	10	220	4
D2810-1-09	0.22	43	0.005	0.0496	0.0055	0.2512	0.0222	0.0378	0.0011	176	241	228	18	239	7
D2810-1-10	77	663	0.116	0.0669	0.0020	1.4614	0.0427	0.1574	0.0016	835	63	915	18	942	9
D2810-1-11	0.22	54	0.004	0.0535	0.0054	0.2585	0.0198	0.0377	0.0009	350	228	233	16	238	6
D2810-1-12	1	171	0.006	0.0499	0.0034	0.2546	0.0163	0.0374	0.0006	187	159	230	13	237	4
D2810-1-13	0.25	70	0.004	0.0485	0.0046	0.2536	0.0208	0.0382	0.0008	124	207	229	17	241	5
D2810-1-14	0.73	76	0.010	0.0486	0.0046	0.2464	0.0202	0.0379	0.0009	128	211	224	16	240	6
D2810-1-15	244	677	0.360	0.0690	0.0016	1.4340	0.0333	0.1494	0.0015	899	48	903	14	898	9
D2810-1-16	106	394	0.270	0.0686	0.0022	1.3945	0.0471	0.1461	0.0017	887	66	887	20	879	10
D2810-1-17	0.37	57	0.006	0.0549	0.0059	0.2698	0.0235	0.0380	0.0010	406	241	243	19	240	6
D2810-1-18	1.02	78	0.013	0.0529	0.0049	0.2645	0.0223	0.0380	0.0009	328	211	238	18	240	5
D2810-1-19	1.18	180	0.007	0.0509	0.0036	0.2519	0.0162	0.0361	0.0007	239	165	228	13	229	4
D2810-1-20	2.34	240	0.010	0.0476	0.0024	0.2458	0.0115	0.0379	0.0005	80	115	223	9	240	3
D2810-1-21	0.51	85	0.006	0.0494	0.0048	0.2444	0.0210	0.0376	0.0007	165	211	222	17	238	5
D2810-1-22	1,517	220	6.909	0.0603	0.0027	0.6598	0.0300	0.0788	0.0011	617	96	514	18	489	7
D2810-1-23	213	157	1.357	0.0566	0.0026	0.6338	0.0281	0.0812	0.0010	476	102	498	17	503	6
D2810-1-24	171	564	0.302	0.0693	0.0021	1.3974	0.0423	0.1451	0.0015	909	56	888	18	873	8
D2810-1-25	0.30	82	0.004	0.0526	0.0053	0.2648	0.0258	0.0373	0.0007	309	230	239	21	236	4
D2810-1-26	0.33	76	0.004	0.0504	0.0057	0.2520	0.0250	0.0370	0.0007	213	244	228	20	235	5
D2810-1-27	62	103	0.603	0.1069	0.0041	4.4798	0.1601	0.3009	0.0036	1747	70	1727	30	1,696	18
D2810-1-28	0.42	89	0.005	0.0520	0.0046	0.2522	0.0192	0.0374	0.0008	287	199	228	16	237	5
D2810-1-29	0.41	74	0.006	0.0543	0.0044	0.2763	0.0191	0.0379	0.0008	383	181	248	15	240	5
D2810-1-30	616	305	2.018	0.0544	0.0026	0.3063	0.0139	0.0406	0.0005	387	112	271	11	256	3
D2810-1-31	134	167	0.805	0.0575	0.0036	0.5664	0.0304	0.0722	0.0010	522	144	456	20	449	6

(Continued on following page)

TABLE 2 (*Continued*) Zircon LA-ICP-MS U-Pb age analysis results for Bangbing eclogites and their surrounding Grt-Ph schists.

Sample spot	Content ($\times10^{-6}$)		Th/U	Isotope ratio						Age/Ma					
	Th	U		$^{207}Pb/^{206}Pb$	1sigma	$^{207}Pb/^{235}U$	1sigma	$^{206}Pb/^{238}U$	1sigma	$^{207}Pb/^{206}Pb$	1sigma	$^{207}Pb/^{235}U$	1sigma	$^{206}Pb/^{238}U$	1sigma
D2810-1-32	0.79	146	0.005	0.0499	0.0036	0.2566	0.0177	0.0376	0.0007	191	167	232	14	238	4
D2810-1-33	1.12	153	0.007	0.0468	0.0034	0.2422	0.0157	0.0380	0.0006	43	163	220	13	241	4
D2810-1-34	238	358	0.664	0.0766	0.0021	1.8410	0.0524	0.1731	0.0018	1,122	54	1,060	19	1,029	10
D2810-1-35	82	245	0.333	0.1673	0.0051	10.8362	0.3519	0.4669	0.0070	2531	50	2509	30	2470	31
D2810-1-36	2.65	265	0.010	0.0517	0.0027	0.2668	0.0134	0.0377	0.0005	272	119	240	11	238	3
D2810-1-37	0.15	44.2	0.003	0.0570	0.0059	0.2857	0.0240	0.0381	0.0010	500	231	255	19	241	6
D2810-1-38	0.40	110	0.004	0.0485	0.0036	0.2388	0.0165	0.0360	0.0006	120	180	217	14	228	4
D2810-1-39	1.11	171	0.006	0.0510	0.0029	0.2629	0.0135	0.0376	0.0006	243	131	237	11	238	4
D2810-1-40	0.49	103	0.005	0.0544	0.0037	0.2811	0.0172	0.0380	0.0007	387	152	252	14	241	4
D2810-2 Grt-Ph schist															
D2810-2-01	187	448	0.42	0.0704	0.0021	1.2245	0.0401	0.1253	0.0022	940	66	812	18	761	13
D2810-2-02	216	319	0.67	0.0735	0.0022	1.4090	0.0484	0.1381	0.0026	1,028	62	893	20	834	15
D2810-2-03	60	191	0.32	0.0638	0.0028	0.8387	0.0381	0.0947	0.0019	744	93	618	21	583	11
D2810-2-04	314	416	0.75	0.0636	0.0019	1.0692	0.0323	0.1216	0.0015	728	64	738	16	740	9
D2810-2-05	616	1,119	0.55	0.0723	0.0015	1.4092	0.0347	0.1402	0.0022	994	42	893	15	846	12
D2810-2-06	235	561	0.42	0.0599	0.0017	0.7163	0.0204	0.0866	0.0011	611	31	548	12	536	7
D2810-2-07	184	541	0.34	0.0656	0.0016	1.1324	0.0293	0.1242	0.0014	794	58	769	14	754	8
D2810-2-08	221	311	0.71	0.0625	0.0019	0.8808	0.0276	0.1017	0.0013	692	71	641	15	624	8
D2810-2-09	333	430	0.78	0.0577	0.0018	0.5809	0.0180	0.0730	0.0010	517	66	465	12	454	6
D2810-2-10	72	594	0.12	0.0586	0.0018	0.6826	0.0245	0.0832	0.0015	554	69	528	15	515	9
D2810-2-11	346	316	1.10	0.0698	0.0021	1.5852	0.0460	0.1645	0.0023	920	61	964	18	981	13
D2810-2-12	311	633	0.49	0.0691	0.0019	1.1746	0.0366	0.1224	0.0023	902	61	789	17	745	13
D2810-2-13	680	1,163	0.58	0.0767	0.0018	1.8710	0.0452	0.1752	0.0026	1,115	14	1,071	16	1,041	14
D2810-2-14	349	282	1.24	0.0723	0.0027	1.2518	0.0469	0.1245	0.0019	994	108	824	21	756	11
D2810-2-15	231	375	0.62	0.0713	0.0020	1.6784	0.0513	0.1688	0.0027	965	64	1,000	19	1,006	15
D2810-2-16	129	481	0.27	0.0748	0.0021	1.8317	0.0505	0.1768	0.0025	1,065	57	1,057	18	1,049	14
D2810-2-17	563	383	1.47	0.0609	0.0020	0.7019	0.0232	0.0833	0.0014	635	72	540	14	516	8
D2810-2-18	117	545	0.22	0.0754	0.0021	1.3526	0.0402	0.1286	0.0019	1,080	57	869	17	780	11
D2810-2-19	221	508	0.43	0.0727	0.0022	1.3126	0.0449	0.1290	0.0023	1,006	62	851	20	782	13
D2810-2-20	295	367	0.80	0.1059	0.0023	4.1912	0.0939	0.2839	0.0032	1729	34	1,672	18	1,611	16
D2810-2-21	191	565	0.34	0.0665	0.0018	0.9087	0.0247	0.0987	0.0015	833	54	656	13	606	9
D2810-2-22	170	650	0.26	0.0777	0.0018	1.8882	0.0447	0.1748	0.0022	1,140	45	1,077	16	1,039	12
D2810-2-23	102	291	0.35	0.0796	0.0023	2.0262	0.0553	0.1847	0.0025	1,187	57	1,124	19	1,093	14

(Continued on following page)

TABLE 2 (*Continued*) Zircon LA-ICP-MS U-Pb age analysis results for Bangbing eclogites and their surrounding Grt-Ph schists.

Sample spot	Content ($\times10^{-6}$)		Th/U	Isotope ratio						Age/Ma					
	Th	U		$^{207}Pb/^{206}Pb$	1sigma	$^{207}Pb/^{235}U$	1sigma	$^{206}Pb/^{238}U$	1sigma	$^{207}Pb/^{206}Pb$	1sigma	$^{207}Pb/^{235}U$	1sigma	$^{206}Pb/^{238}U$	1sigma
D2810-2-24	92	323	0.28	0.1021	0.0025	3.5831	0.0904	0.2527	0.0032	1,665	46	1,546	20	1,452	16
D2810-2-25	150	232	0.65	0.0684	0.0027	1.1885	0.0475	0.1260	0.0020	880	84	795	22	765	11
D2810-2-26	523	1,075	0.49	0.0613	0.0019	0.6698	0.0205	0.0791	0.0011	650	69	521	12	491	7
D2810-2-27	339	664	0.51	0.0750	0.0022	1.5477	0.0458	0.1488	0.0020	1,133	58	950	18	894	11
D2810-2-28	397	386	1.03	0.0831	0.0025	1.9986	0.0693	0.1720	0.0028	1,272	59	1,115	23	1,023	15
D2810-2-29	77	1,378	0.06	0.0732	0.0019	1.2824	0.0358	0.1263	0.0017	1,020	54	838	16	767	10
D2810-2-30	577	1701	0.34	0.0687	0.0016	1.1302	0.0265	0.1188	0.0015	889	81	768	13	724	9
D2810-2-31	468	668	0.70	0.1041	0.0022	3.7809	0.0808	0.2630	0.0037	1,698	40	1,589	17	1,505	19
D2810-2-32	524	412	1.27	0.1638	0.0034	8.7129	0.1962	0.3831	0.0052	2495	35	2308	21	2091	24
D2810-2-33	224	931	0.24	0.0863	0.0017	2.7471	0.0597	0.2289	0.0028	1,346	39	1,341	16	1,329	15
D2810-2-34	89	918	0.10	0.0913	0.0019	2.5343	0.0573	0.2002	0.0030	1,454	39	1,282	16	1,176	16
D2810-2-35	487	508	0.96	0.0588	0.0019	0.7151	0.0227	0.0879	0.0012	561	70	548	13	543	7
D2810-2-36	486	1,051	0.46	0.0680	0.0016	1.1623	0.0289	0.1231	0.0016	878	50	783	14	748	9
D2810-2-37	211	302	0.70	0.0674	0.0022	1.3508	0.0442	0.1455	0.0023	850	64	868	19	875	13
D2810-2-38	151	258	0.58	0.0707	0.0019	1.7297	0.0504	0.1759	0.0026	950	56	1,020	19	1,045	14
D2810-2-39	329	535	0.61	0.1024	0.0023	4.1094	0.0945	0.2887	0.0037	1,678	42	1,656	19	1,635	18
D2810-2-40	947	746	1.27	0.0823	0.0021	2.0991	0.0565	0.1832	0.0026	1,254	18	1,149	19	1,084	14
D2810-2-41	226	287	0.79	0.0978	0.0027	3.7252	0.1074	0.2740	0.0043	1,583	51	1,577	23	1,561	22
D2810-2-42	444	400	1.11	0.0807	0.0022	2.1071	0.0590	0.1893	0.0033	1,215	59	1,151	19	1,118	18
D2810-2-43	230	284	0.81	0.0706	0.0021	1.6494	0.0481	0.1695	0.0026	946	61	989	18	1,009	14
D2810-2-44	186	394	0.47	0.0689	0.0023	1.1767	0.0405	0.1236	0.0021	895	67	790	19	751	12
D2810-2-45	351	622	0.56	0.0740	0.0019	1.7915	0.0552	0.1742	0.0037	1,043	55	1,042	20	1,035	20
D2810-2-46	387	782	0.50	0.0728	0.0017	1.5746	0.0376	0.1558	0.0022	1,009	46	960	15	933	12
D2810-2-47	419	1,109	0.38	0.0985	0.0019	3.2800	0.0664	0.2398	0.0030	1,596	36	1,476	16	1,386	15
D2810-2-48	873	775	1.13	0.0700	0.0017	1.3251	0.0340	0.1363	0.0019	929	49	857	15	824	11
D2810-2-49	430	552	0.78	0.0722	0.0017	1.4216	0.0346	0.1425	0.0020	991	49	898	15	859	11
D2810-2-50	453	560	0.81	0.0823	0.0022	2.1536	0.0630	0.1884	0.0028	1,254	19	1,166	20	1,113	15
D2810-2-51	212	605	0.35	0.0711	0.0017	1.4084	0.0332	0.1432	0.0017	961	49	892	14	863	10
D2810-2-52	98	1,218	0.08	0.0659	0.0016	1.1829	0.0271	0.1301	0.0017	1,200	51	793	13	789	10
D2810-2-53	176	635	0.28	0.0716	0.0018	1.6708	0.0476	0.1686	0.0031	976	55	998	18	1,004	17
D2810-2-54	176	222	0.79	0.0675	0.0024	1.4834	0.0506	0.1605	0.0025	854	68	924	21	960	14
D2810-2-55	199	463	0.43	0.0773	0.0020	1.6585	0.0450	0.1552	0.0022	1,128	58	993	17	930	12
	673	909	0.74	0.3240	0.0068	31.1132	0.7165	0.6936	0.0102	3,591	32	3,523	23	3,396	39

(Continued on following page)

TABLE 2 (*Continued*) Zircon LA-ICP-MS U-Pb age analysis results for Bangbing eclogites and their surrounding Grt-Ph schists.

Sample spot	Content ($\times10^{-6}$)		Th/U	Isotope ratio						Age/Ma					
	Th	U		$^{207}Pb/^{206}Pb$	1sigma	$^{207}Pb/^{235}U$	1sigma	$^{206}Pb/^{238}U$	1sigma	$^{207}Pb/^{206}Pb$	1sigma	$^{207}Pb/^{235}U$	1sigma	$^{206}Pb/^{238}U$	1sigma
D2810-2-56															
D2810-2-57	97	1,553	0.06	0.0591	0.0016	0.6282	0.0182	0.0767	0.0012	569	62	495	11	476	7
D2810-2-58	442	479	0.92	0.0639	0.0020	0.9305	0.0289	0.1059	0.0017	739	264	668	15	649	10
D2810-2-59	623	682	0.91	0.1002	0.0023	3.9074	0.0982	0.2820	0.0043	1,628	43	1,615	20	1,601	22
D2810-2-60	119	209	0.57	0.0882	0.0024	2.7151	0.0733	0.2234	0.0031	1,387	19	1,333	20	1,300	17
D2810-2-61	701	815	0.86	0.0606	0.0019	0.6961	0.0230	0.0835	0.0015	633	73	536	14	517	9
D2810-2-62	185	278	0.66	0.0711	0.0021	1.5028	0.0474	0.1539	0.0023	961	61	932	19	923	13
D2810-2-63	75	124	0.61	0.1147	0.0034	4.5940	0.1365	0.2911	0.0041	1876	54	1748	25	1,647	21
D2810-2-64	131	359	0.37	0.0681	0.0019	1.4591	0.0410	0.1553	0.0020	872	57	914	17	930	11
D2810-2-65	904	1,018	0.89	0.0806	0.0017	2.1972	0.0482	0.1967	0.0023	1,213	41	1,180	15	1,158	13
D2810-2-66	847	853	0.99	0.0730	0.0018	1.4341	0.0336	0.1430	0.0019	1,013	48	903	14	862	10
D2810-2-67	326	395	0.83	0.0932	0.0024	2.3825	0.0702	0.1849	0.0033	1,492	49	1,237	21	1,094	18
D2810-2-68	212	626	0.34	0.0695	0.0018	1.1808	0.0312	0.1234	0.0019	922	53	792	15	750	11
D2810-2-69	187	190	0.98	0.0630	0.0025	1.0185	0.0451	0.1158	0.0019	709	84	713	23	706	11
D2810-2-70	145	376	0.38	0.0876	0.0023	2.1524	0.0576	0.1781	0.0024	1,373	56	1,166	19	1,057	13
D2810-2-71	43	436	0.10	0.2729	0.0053	24.1833	0.5147	0.6403	0.0083	3,323	30	3,276	21	3,190	33
D2810-2-72	93	1,171	0.08	0.0673	0.0018	1.1045	0.0318	0.1182	0.0016	856	54	756	15	720	9
D2810-2-73	186	690	0.27	0.1643	0.0037	9.3819	0.2442	0.4134	0.0072	2502	38	2376	24	2230	33
D2810-2-74	301	582	0.52	0.1043	0.0026	3.7635	0.0947	0.2618	0.0036	1702	45	1,585	20	1,499	18
D2810-2-75	126	374	0.34	0.0648	0.0021	1.1655	0.0436	0.1300	0.0024	769	69	785	20	788	14
D2810-2-76	140	219	0.64	0.0747	0.0027	1.5589	0.0567	0.1521	0.0023	1,061	79	954	23	913	13
D2810-2-77	375	573	0.66	0.1007	0.0022	3.7950	0.0861	0.2723	0.0033	1,639	41	1,592	18	1,553	17
D2810-2-78	252	255	0.99	0.0618	0.0025	0.7277	0.0292	0.0863	0.0014	733	82	555	17	534	9
D2810-2-79	90	153	0.58	0.0757	0.0028	1.7338	0.0645	0.1670	0.0027	1,087	74	1,021	24	995	15
D2810-2-80	796	866	0.92	0.0857	0.0018	2.6439	0.0608	0.2226	0.0030	1,331	36	1,313	17	1,296	16
D2810-2-81	113	168	0.67	0.0820	0.0024	2.3465	0.0722	0.2073	0.0030	1,256	58	1,226	22	1,215	16
D2810-2-82	171	355	0.48	0.0732	0.0020	1.8535	0.0537	0.1843	0.0031	1,020	56	1,065	19	1,090	17
D2810-2-83	555	1,114	0.50	0.0769	0.0018	1.9594	0.0510	0.1839	0.0027	1,120	46	1,102	18	1,088	15
D2810-2-84	126	249	0.50	0.0736	0.0021	1.6877	0.0463	0.1672	0.0025	1,031	58	1,004	18	997	14
D2810-2-85	822	514	1.60	0.0759	0.0020	1.7696	0.0472	0.1689	0.0023	1,094	54	1,034	17	1,006	13
D2810-2-86	244	149	1.63	0.0754	0.0028	1.9517	0.0705	0.1899	0.0033	1,080	73	1,099	24	1,121	18
D2810-2-87	234	176	1.33	0.0665	0.0032	0.7933	0.0370	0.0870	0.0015	833	100	593	21	538	9
	93	227	0.41	0.0717	0.0028	1.3924	0.0583	0.1404	0.0026	989	81	886	25	847	15

(Continued on following page)

TABLE 2 (*Continued*) Zircon LA-ICP-MS U-Pb age analysis results for Bangbing eclogites and their surrounding Grt-Ph schists.

Sample spot	Content ($\times 10^{-6}$)		Th/ U	Isotope ratio						Age/Ma					
	Th	U		$^{207}Pb/^{206}Pb$	1sigma	$^{207}Pb/^{235}U$	1sigma	$^{206}Pb/^{238}U$	1sigma	$^{207}Pb/^{206}Pb$	1sigma	$^{207}Pb/^{235}U$	1sigma	$^{206}Pb/^{238}U$	1sigma
D2810-2-88															
D2810-2-89	311	491	0.63	0.0763	0.0022	1.7947	0.0518	0.1702	0.0025	1,102	51	1,044	19	1,013	14

TABLE 3 Zircon LA-ICP-MS trace element (ppm) analyses for Bangbing eclogites.

Sample spot	Y	Nb	Ta	La	Ce	Pr	Nd	Sm	Eu	Gd	Tb	Dy	Ho	Er	Tm	Yb	Lu	Ti	*T*°C	δEu
D2810-1-01	63	0.11	0.01	dd	0.13	dd	0.02	0.45	0.48	4.77	1.50	9.80	2.04	5.18	0.84	5.73	1.13	4.15	670	1.01
D2810-1-02	54	0.22	0.05	dd	0.17	dd	dd	0.06	0.16	2.51	0.86	7.34	1.77	4.64	0.70	4.78	0.82	1.26	582	1.19
D2810-1-03	47	0.16	0.03	dd	0.09	dd	dd	0.14	0.45	3.72	1.01	7.52	1.52	3.92	0.58	4.45	0.97	3.29	651	1.88
D2810-1-04	69	0.23	0.03	dd	0.26	dd	dd	0.06	0.28	3.18	1.11	10.08	2.18	6.06	0.81	5.42	0.98	2.55	632	1.98
D2810-1-05	1,187	2.64	0.92	0.01	12.51	0.05	1.05	2.73	1.01	17.47	6.58	92.52	40.07	192.52	44.45	436.93	99.06	11.73	761	0.45
D2810-1-06	85	0.19	0.03	dd	0.18	dd	0.08	0.12	0.35	3.49	1.23	11.42	2.93	9.01	1.36	10.52	1.99	4.08	668	1.68
D2810-1-07	52	0.09	0.02	0.01	0.08	dd	dd	0.18	0.43	5.18	1.26	8.96	1.65	4.22	0.60	5.10	0.87	1.14	576	1.39
D2810-1-08	50	0.13	0.01	0.15	dd	0.03	0.12	0.28	3.53	0.96	7.57	1.75	4.51	0.67	5.39	0.99	0.03	2.49	630	1.33
D2810-1-09	33	0.09	dd	0.07	dd	dd	0.24	0.20	2.62	0.85	5.19	1.01	2.72	0.39	3.42	0.72	0.04	1.15	576	0.79
D2810-1-10	826	1.90	1.23	dd	2.37	0.03	0.88	3.20	0.11	17.38	6.99	80.47	28.43	118.49	24.72	220.97	45.09	15.24	787	0.04
D2810-1-11	60	0.10	0.03	dd	0.14	dd	dd	0.33	0.32	4.04	1.16	8.32	1.94	5.58	0.84	6.25	1.26			0.84
D2810-1-12	56	0.16	0.04	dd	0.16	dd	dd	0.40	0.32	3.52	1.15	7.82	1.68	4.81	0.69	4.02	0.99	3.92	665	0.83
D2810-1-13	49	0.17	0.02	dd	0.11	dd	0.02	0.26	0.27	3.20	1.01	6.83	1.44	4.29	0.79	6.14	1.19	5.68	695	0.93
D2810-1-14	92	0.12	0.01	dd	0.09	dd	dd	0.15	0.34	2.67	1.16	11.06	2.85	8.65	1.40	9.48	2.08	2.90	642	1.65
D2810-1-15	1,327	9.90	4.75	dd	15.95	0.05	1.43	3.91	0.09	24.84	9.30	117.87	47.57	218.91	44.78	395.07	76.69	5.07	686	0.03
D2810-1-16	124	1.23	0.67	0.01	1.07	0.02	0.86	2.25	0.05	11.08	2.81	20.08	4.22	11.84	1.97	14.16	2.68	9.24	739	0.03
D2810-1-17	47	0.12	0.02	dd	0.08	dd	dd	0.08	0.09	1.96	0.56	5.22	1.49	4.42	0.61	4.59	0.83	1.31	585	0.70
D2810-1-18	83	0.18	0.02	dd	0.14	dd	0.05	0.20	0.20	2.96	1.21	9.78	2.46	7.98	1.19	7.72	1.67	3.51	656	0.78
D2810-1-19	54	0.20	0.04	dd	0.13	dd	0.06	0.20	0.37	2.82	1.05	7.57	1.80	5.15	0.79	5.58	1.16	2.24	622	1.50
D2810-1-20	66	0.14	0.04	dd	0.25	dd	0.03	0.26	0.36	3.31	1.11	9.00	2.00	5.82	0.78	4.62	0.82	4.10	669	1.19
D2810-1-21	100	0.12	0.02	dd	0.13	dd	0.05	0.24	0.32	3.62	1.38	12.34	3.36	9.18	1.32	9.45	1.88	0.63	539	1.04
D2810-1-22	1773	3.58	0.71	0.51	254.02	3.04	43.30	47.69	20.37	130.58	28.29	231.55	64.65	226.15	39.67	317.48	57.89	19.15	811	0.79
D2810-1-23	699	1.97	0.97	0.01	36.25	0.16	3.26	5.87	1.05	24.10	6.71	73.64	24.10	101.67	20.24	170.90	33.55	3.14	647	0.27
D2810-1-24	771	0.78	0.63	0.04	2.28	0.19	3.07	6.73	0.20	38.93	10.63	93.69	26.46	95.00	16.47	129.91	24.27	6.44	706	0.04
D2810-1-25	120	0.16	0.04	dd	0.12	dd	dd	0.18	0.40	3.86	1.59	14.26	3.77	11.59	1.67	11.89	2.38	1.57	597	1.47
D2810-1-26	84	0.13	0.03	dd	0.07	dd	0.02	0.26	0.28	3.12	1.19	10.25	2.48	8.21	1.21	8.50	1.83	3.02	645	0.94
D2810-1-27	469	1.12	0.68	dd	12.83	0.02	0.91	2.21	0.61	8.65	3.20	40.36	15.25	72.07	16.01	158.15	36.29	6.42	706	0.42
D2810-1-28	65	0.17	0.05	dd	0.10	dd	0.05	0.27	0.26	2.91	0.96	8.28	2.11	5.97	0.85	6.87	1.37	1.64	601	0.90
D2810-1-29	71	0.13	0.04	dd	0.11	dd	0.02	0.22	0.27	3.25	1.09	8.56	2.14	6.49	0.89	6.89	1.44	3.34	652	0.97
D2810-1-30	1,460	3.69	0.81	0.01	119.81	0.21	4.22	7.49	3.32	42.78	12.71	140.35	50.56	220.25	43.95	398.08	81.64	3.98	666	0.57
D2810-1-31	677	1.10	0.68	dd	14.94	0.06	0.95	2.15	0.46	12.98	4.83	56.58	22.54	104.40	21.69	197.62	41.57	10.52	751	0.27
D2810-1-32	70	0.11	0.05	0.01	0.11	dd	0.02	0.22	0.30	3.85	1.10	9.23	2.27	6.78	0.95	5.62	1.24	1.96	613	0.98
D2810-1-33	58	0.20	0.03	dd	0.13	dd	dd	0.22	0.23	3.00	0.85	7.93	1.91	5.17	0.68	4.96	0.91	1.73	604	0.85
D2810-1-34	596	2.66	1.84	0.02	15.38	0.11	1.27	3.00	0.11	14.39	4.62	54.40	21.21	91.76	18.81	17dd	32.86	3.78	662	0.05
D2810-1-35	374	0.83	0.47	0.02	7.51	0.07	1.06	1.41	0.39	8.49	2.86	31.20	12.43	57.22	12.42	119.74	28.06	4.48	676	0.35
D2810-1-36	62	0.27	0.05	0.01	0.21	dd	0.02	0.13	0.30	2.60	0.94	8.74	1.97	5.90	0.70	4.33	0.80	3.87	664	1.53
D2810-1-37	27	0.10	0.03	dd	0.06	dd	dd	0.23	0.29	2.45	0.71	3.87	0.84	1.82	0.33	2.52	0.57	2.53	631	1.19
D2810-1-38	56	0.19	0.03	0.01	0.14	dd	dd	0.41	0.31	3.46	1.12	7.40	1.72	4.60	0.68	5.15	1.06	1.75	605	0.79
D2810-1-39	74	0.12	0.03	dd	0.12	dd	0.06	0.35	0.37	4.78	1.41	12.13	2.44	6.69	0.96	7.20	1.54	4.23	671	0.88
D2810-1-40	113	0.09	0.03	dd	0.08	dd	0.02	0.31	0.27	4.18	1.44	13.19	3.58	10.62	1.48	11.42	2.19	0.19	474	0.73

dd indicates below detection limits. T°C according to Ferry and Watson, 2007, by assuming that $\alpha_{TiO2}=\alpha_{SiO2}$.

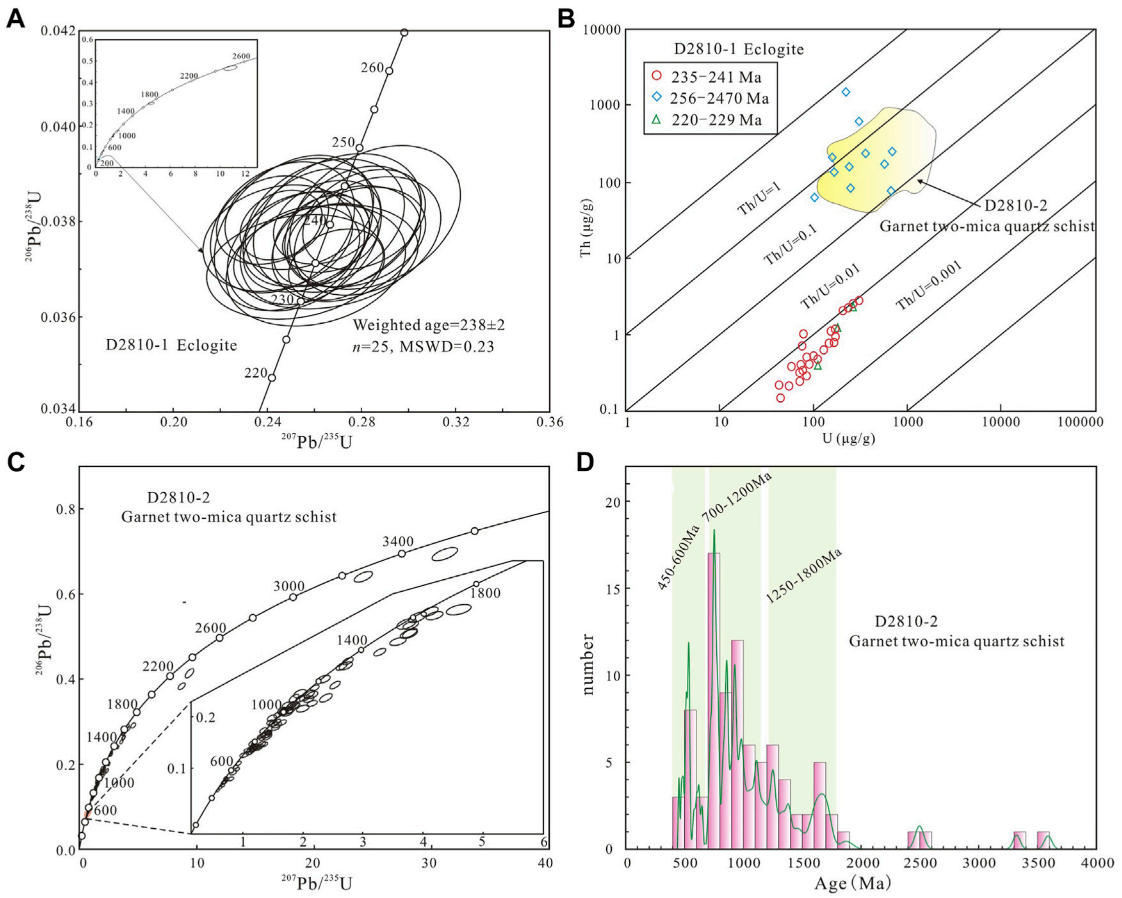

FIGURE 5
Zircon U-Pb ages **(A,C,D)** and Th/U ratios **(B)** for eclogites and Grt-Ph schists.

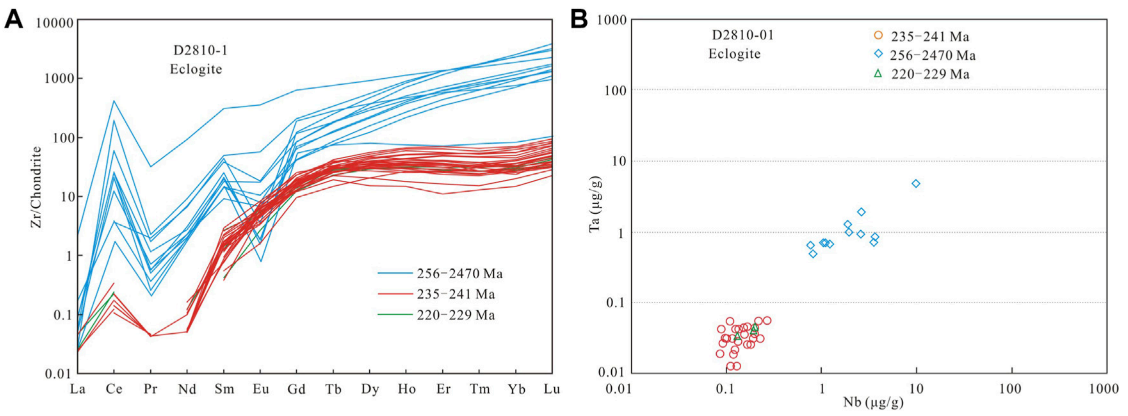

FIGURE 6
REE patterns **(A)** and Nb-Ta contents **(B)** of zircons from Bangbing eclogites.

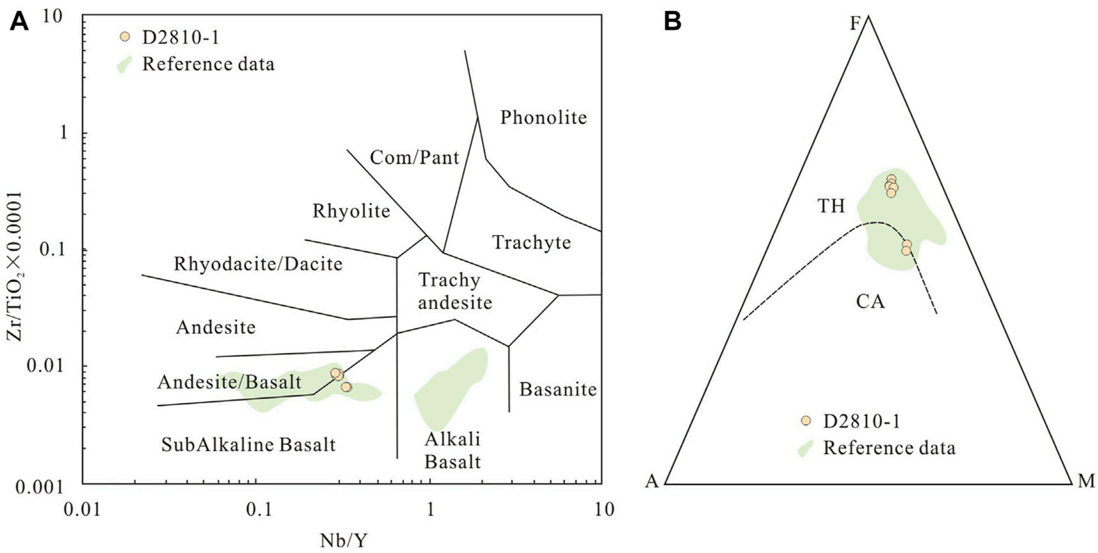

FIGURE 7
Zr/TiO_2-Nb/Y **(A)** and AFM **(B)** illustration for Bangbing eclogites.

TABLE 4 Zircon Lu-Hf isotope analysis results for Bangbing eclogites.

Sample spot	Age (Ma)	$^{176}Yb/^{177}Hf$	1σ	$^{176}Lu/^{177}Hf$	1σ	$^{176}Hf/^{177}Hf$	1σ	$\varepsilon_{Hf}(0)$	$\varepsilon_{Hf}(t)$	t_{DM1} (Ma)	t_{DM2} (Ma)	$f_{Lu/Hf}$
D2810-1												
06	451	0.000539	0.000021	0.000017	0.000001	0.282946	0.000012	6.16	16.10	422	404	−1.00
09	451	0.000420	0.000008	0.000014	0.000001	0.282929	0.000012	5.57	15.51	443	442	−1.00
11	451	0.000426	0.000015	0.000013	0.000001	0.282947	0.000014	6.20	16.14	421	402	−1.00
37	451	0.000407	0.000007	0.000012	0.000001	0.282917	0.000011	5.13	15.07	463	470	−1.00
39	451	0.000521	0.000012	0.000017	0.000001	0.282,905	0.000014	4.70	14.64	480	498	−1.00

diagrams, the sample shows a general pattern of LREE depletion and HREE enrichment gradually (Figure 6A). However, there are obvious differences in REE patterns between the core-rim and non-core-rim structures test spots. (1) ∑REE: high and variable for those with core-rim structures (73–1,465 ppm) and low for those without core-rim structures (14–52 ppm). (2) Enrichment of HREE: HREEs are significantly more abundant in core-rim structures (69–1,096 ppm), with high degrees of fractionation (1.28–25.01). Comparatively, HREEs in non-core-rim structures range from 13 to 51 ppm, with low degrees of fractionation of 0.85–3.55. (3) Eu and Ce anomalies: Eu negative anomalies are more strongly apparent in the non-core-rim than in the core-rim structures (0.03–0.79, mean 0.27; 0.70–1.98, mean 1.14). Conversely, Ce positive anomalies are more obvious in the core-rim structures.

The Y, Nb and Ta contents vary considerably in the zircons with different structures. The Nb and Ta contents and ratios of the test spots in the core-rim structures are much higher than those in the non-core-rim structures. Ti contents range 3.14–19.15 ppm and 0.19–5.68 ppm, respectively, corresponding to formed temperatures of 647–811°C (mean 716°C) and 447–695°C (mean 629°C, excluding 447°C) (calculated after Ferry and Watson, 2007).

Whole-rock Sr-Nd isotope

The results of whole-rock Sr-Nd isotope analysis are shown in Table 1. The eclogite samples have $^{87}Sr/^{86}Sr$ ranging from 0.705797 to 0.712837, mean=0.709334.$^{143}Nd/^{144}Nd$ range from 0.512731 to 0.512773, mean=0.512753 ($^{87}Sr/^{86}Sr$)t range from 0.705392 to 0.712126, mean=0.708387 ($^{143}Nd/^{144}Nd$)t range from 0.512218 to 0.512287, mean=0.5122432. ε_{Nd}(t) values range from 3.14 to 4.49, mean=3.63 (t=451 Ma, Wang et al., 2019).

Zircon Lu-Hf isotope

The locations of the analyzed spots for the single grain zircon Lu-Hf isotope are shown in Figure 4 and their results are

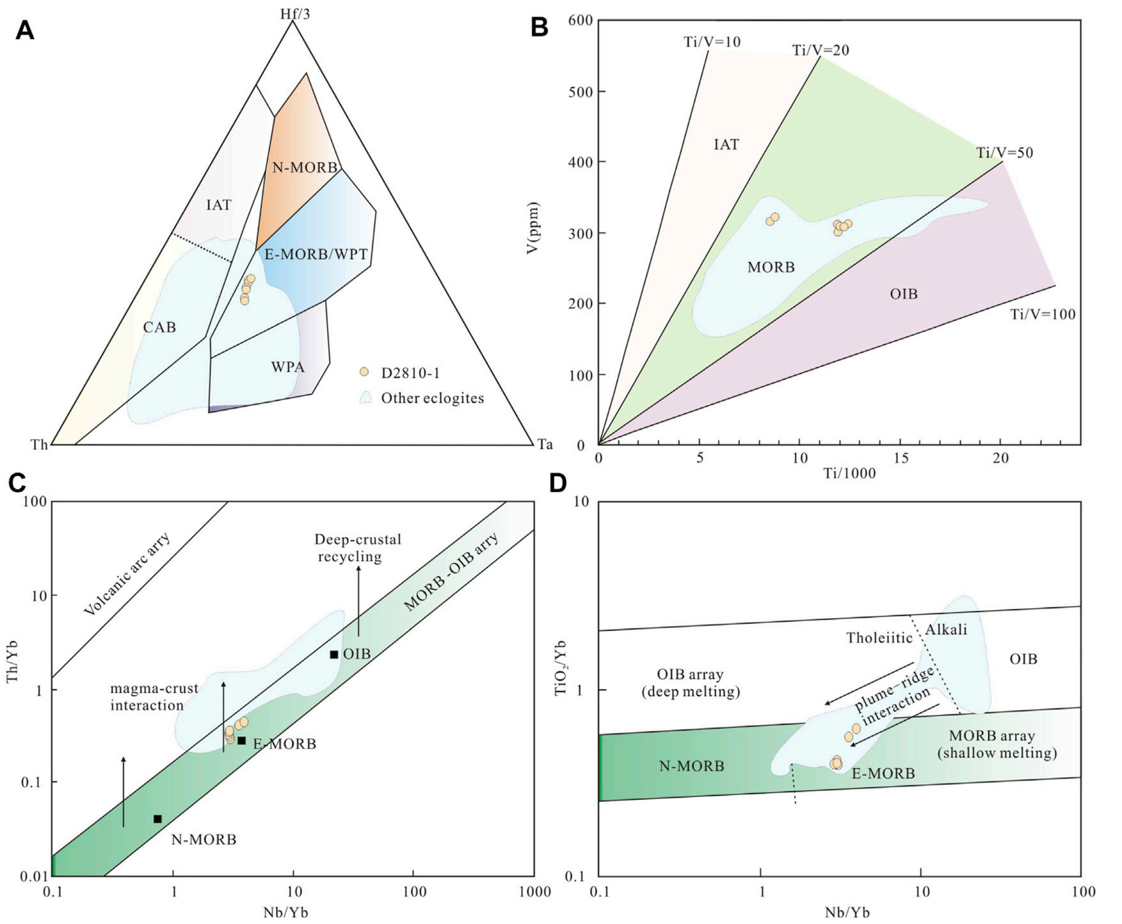

FIGURE 8
Discrimination diagrams of tectonic settings for Bangbing eclogites. **(A)** Hf/3-Th-Ta (after Wood, 1980). **(B)** V-Ti/1,000 (after Shervais, 1982) **(C,D)** Th/Yb-Nb/Yb, and TiO_2/Yb-Nb/Yb (after Pearce, 2008). Other eclogites (after Sun et al., 2017; Wang HN. et al., 2021). N-MORB, normal ocean ridge basalts; E-MORB, enriched mid ocean ridge basalts; OIB, oceanic island basalts; WPA, within-palte alkali basalts; WPT, within-plate tholeiites; WPA, within-plate basalts; IAT, island arc tholeiites; CAB, calc alkaline basalts.

presented in Table 4. Five analyses show low $^{176}Hf/^{177}Hf$ and $^{176}Lu/^{177}Hf$ values of 0.282905–0.282947 and 0.000012 to 0.000017, respectively. $\varepsilon_{Hf}(t)$ values range from 14.64 to 16.14, mean 15.49 (t = 451 Ma, Wang et al., 2019), and their stage II model ages range from 402 to 498 Ma, mean 443 Ma, which is older than zircon U-Pb metamorphic ages.

Discussion

Timing of HP metamorphism

Currently, the eclogites geochronology research in western Yunnan is mainly concentrated in Mengku and Qianmai areas. Sun et al. (2018) concluded from zircon U-Pb chronology of the retrograde eclogites from Daizhai, Kongjiao and Dijie in the Mengku area that 801 Ma is its protolithic age, which is consistent with Rodinia supercontinent initial breakup, and 447 Ma, 291 Ma and 229–227 Ma, respectively, represent the ages at different stages of metamorphism the eclogites have undergone. Wang et al. (2019) proposed 451 Ma as the protolithic age in this area, and 245–246 Ma as the peak metamorphic age. Wang et al. (2021) published the peak metamorphic age of 234–233 Ma for the eclogites in Qianmai area, which represents the timing of continental subduction (Zhao et al., 2021). Previous studies on zircon U-Pb geochronology from the Suyi blueschists yielded protolith ages of 279–260 Ma, and peak metamorphic ages of 214 Ma–242 Ma (Zhao et al., 1994; Fan et al., 2015). The eclogite-facies metamorphism in the LLSZ, which underwent a similar tectonic evolution as CMSZ, occurred at 237, 230 Ma, while continental collision and exhumation occurred at ~220 Ma (Li et al., 2006; Zhang et al., 2010; Zhai et al., 2011, 2017). In the Pianshishan area of central Qiangtang, the eclogites have a

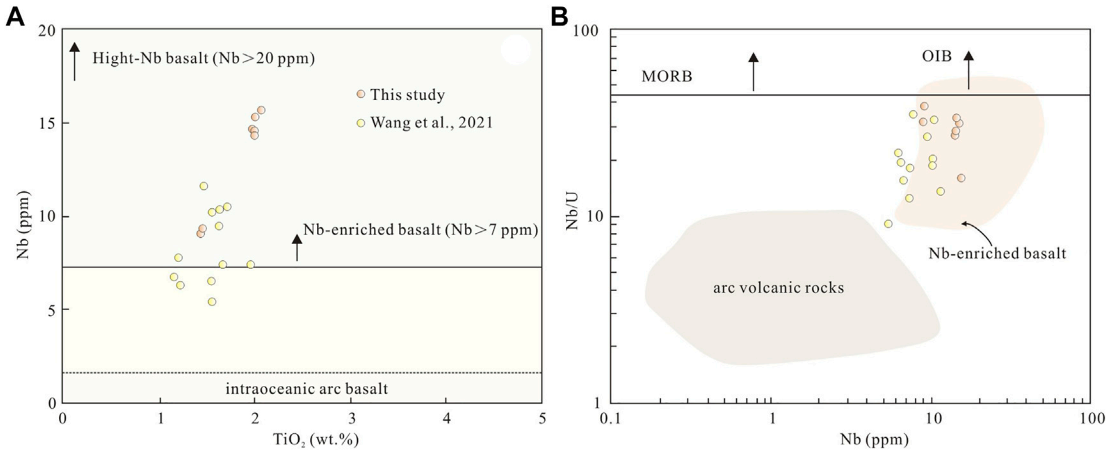

FIGURE 9
TiO_2 vs Nb **(A)** and Nb vs Nb/U **(B)** diagrams for Bangbing eclogites. **(A)**, High-Nb basalt and Nb-enriched data form Sajona et al., 1993, 1996; intra-oceanic arc basalts after Martin et al., 2005; **(B)**, arc volcanic rocks data and Nb-enriched basalts (NEB) data form Kepezhinaskas et al., 1996.

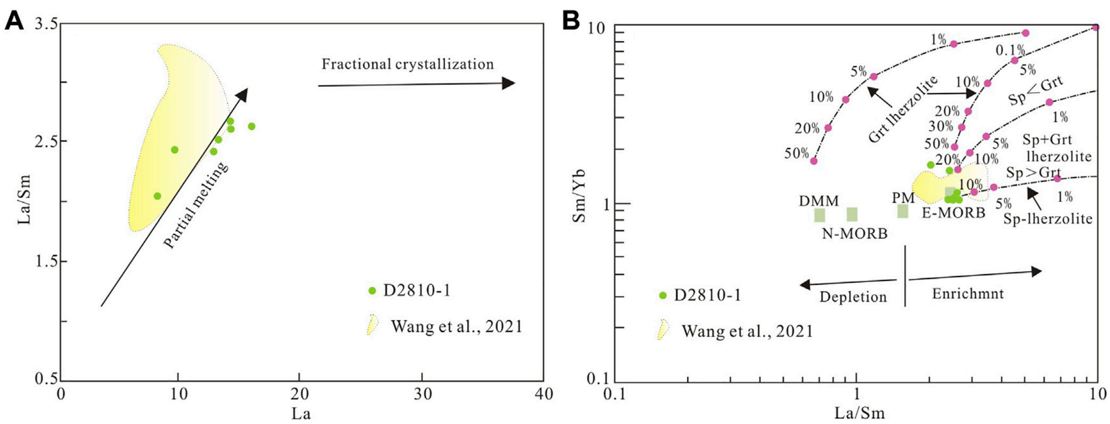

FIGURE 10
La/Sm-La **(A)** and Sm/Yb-La/Sm **(B)** diagrams for Bangbing eclogites. Numbers refer to percentages of melts. DMM, depleted MORB mantle; N-MORB, normal MORB; E-MORB, ecriched MORB; PM, primitive mantle.

protolithic age of 238 Ma, a peak metamorphic age of ~233 Ma and an outcrop age of ~220 Ma, which is considered to be a rare rapid subduction and exhumation evolution.

As shown above, the morphology and cathodoluminescence of the zircons in the Bangbing eclogites are consistent with a metamorphic origin (Figure 4A, Wu and Zheng, 2004). Twenty-five analyses (Group Ⅱ) in the zircon yield concentrated ages from 235 to 241 Ma, with $^{206}Pb/^{238}U$ weighted mean ages of 238 ± 2 Ma (MSWD=0.23). U and Th in zircons show low values of 0.15–2.83 and 43 × 10^{-6}–304 ppm, respectively, with Th/U ratios of 0.004–0.01, much less than 0.1. Zircons REE distribution patterns exhibit excellent agreement (Figure 6A). The above characteristics all suggest that these zircons were grown in the same environment. Enrichment of HREE relative to LREE, slight positive Ce anomaly, and weak Eu anomaly suggest the absence of feldspar, and support that these zircons was not produced from magmatic conditions (Rubatto, 2002; Sun et al., 2002). The high enrichment of HREE in the garnets causes a reduction in the zircons formed simultaneously with these garnets. Accordingly, metamorphic zircons grown in equilibrium with garnets are characterized by low ∑REE, with their HREE contents showing depletion compared to zircons of other origins (Wu et al., 2002; Hofmnn, 1988). Rutile, a widespread UHP-HP metamorphic mineral in eclogites, is highly enriched in HFSEs, especially Nb and Ta, and has high Nb/Ta ratios (Rudnicketal., 2000). Thus, low Nb and Ta content characteristics in metamorphic zircons are the

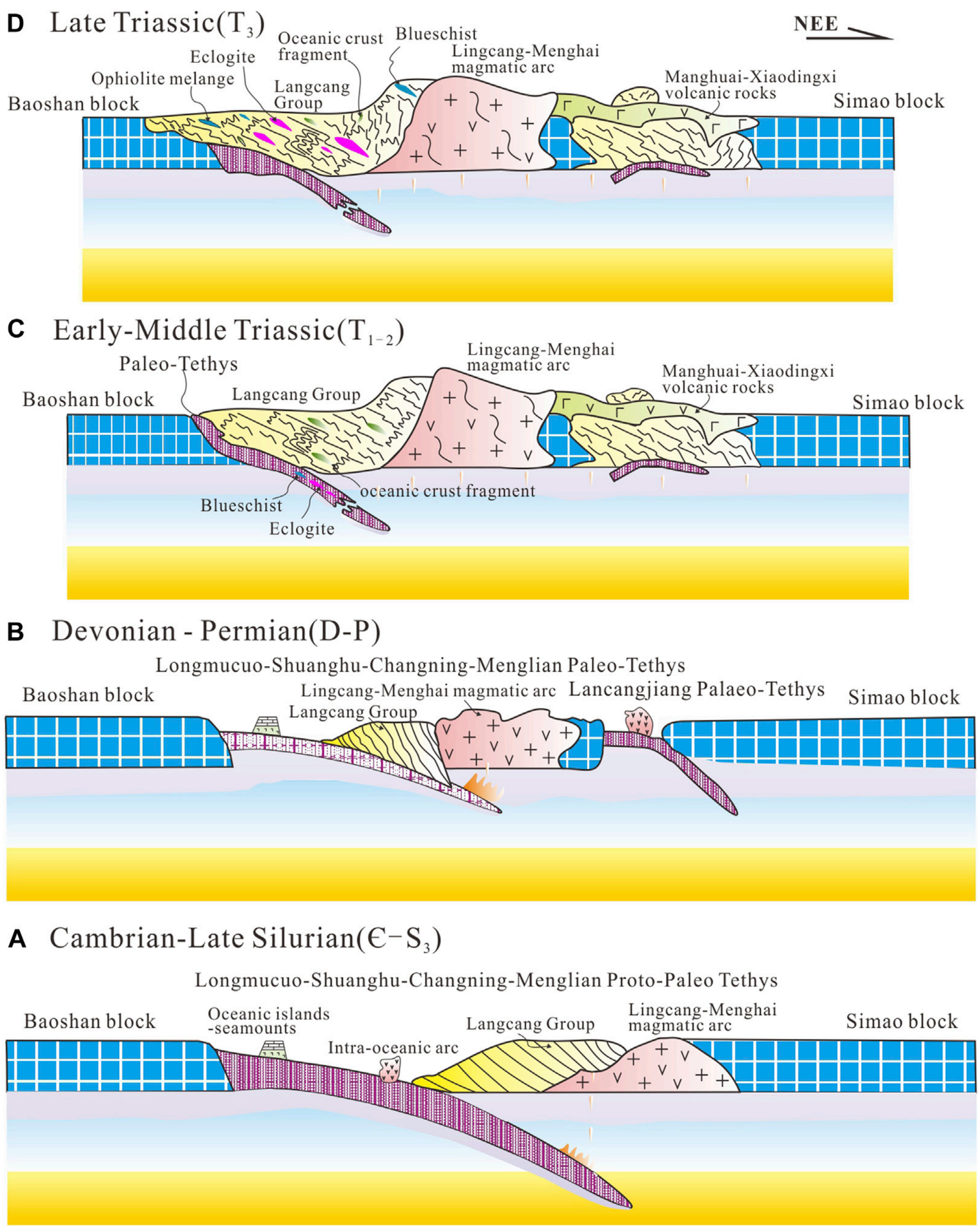

FIGURE 11
Model for the tectonic evolution of the Proto-Paleo Tethys in Changning-Menglian suture zone. **(A)**, Eastward subduction of the Proto-Tethys Ocean during the Late Paleozoic. **(B)**, Extended and subducted of the Paleo-Tethys Ocean during the Devonian and Early Carboniferous-Late Permian periods. **(C)**, Large-scale subduction of the Paleo-Tethys Ocean during the Early-Middle Triassic. **(D)**, the Changning-Menglian Ocean closed and the arc-continent and continent-continent collision orogeny in the Late Triassic. And final uplift of HP/UHP rocks.

result of equilibrium crystallization with rutile (Li et al., 2004). In this study the zircons show this typical REE distribution patterns (Figure 6A), while zircons in the samples have low Nb and Ta contents (0.089–0.27 ppm, 0.012–0.053 ppm) and significantly lower Nb/Ta ratios than magmatic zircons (Figure 6B). It is indicated that these zircons all crystallised in equilibrium with garnets and rutiles and formed during the eclogite-facies metamorphism, with weighted average ages most closely matching the peak metamorphic ages. The zircon Ti thermometer calculations of 539–695°C (mean 629°C, Table 3) are in general agreement with the regional peak metamorphic temperature of the eclogites (Sun et al., 2019; Wang et al., 2020b; Wang HN. et al., 2021; Fu et al., 2021). It further supports that 238 Ma should be the peak metamorphic age. 220–229 Ma are probably the ages of exhumation. Other older values are captured ages.

The general characteristics of zircons in the surrounding Grt-Ph-Qz schists differ from those in the eclogites, with the youngest group of ages peaking around 450–600 Ma, suggesting that the metasedimentary rocks may have been deposited as recently as Early Paleozoic (Wang et al., 2018; Peng et al., 2020b).

Origin of protolith

The eclogite protoliths have undergone multi-phase complex metamorphic alteration, subject to fluids, recrystallization and accountings, resulting in large variations in the LILEs such as Sr and Pb (Becker et al., 1999). The HFSEs (e.g., Na, Ta, Ti, Hf, etc.) and some major elements (e.g., TiO_2, P_2O_5, Al_2O_3) remain less mobile during metamorphism and are believed to reflect their protolith compositions (Hou et al., 1996). SiO_2 contents of the Bangbing eclogites range from 45.92 to 50.59%, showing basaltic characteristics. TiO_2 values of 1.28%–2.01% (mean 1.61%) are higher than those of intraplate basalts (1.00%, Condie, 1989) and ocean island basalts (OIBs, 0.64%, Condie, 1989), and similar to normal mid-ocean ridge basalts (N-MORBs) and mid-ocean ridge tholeiitic basalts (E-MORB, 1.61%, Hofmann, 1988). As the samples were altered to some extent, analysis using anti-alteration elemental diagram (Zr/TiO_2-Nb/Y) showed that the data spots fell in the basaltic-andesite zone and in the subalkaline basaltic zone (Figure 7A). In the AFM diagram, except for two spots that fall within the boundary zone between calc-alkaline and tholeiitic basalts, all data are mainly classified as tholeiite series (Figure 7B), which is in agreement with the characteristics of the Qiangtang, and Mengku eclogites. Earlier studies have suggested that the protoliths of eclogites in the CMSZ are characterised by E-MORB and also by OIB (Sun et al., 2017; Wang et al., 2021). The results presented here show that the samples are similar to the E-MORB geochemistry in either the total REE and trace element patterns (Figure 3), the Hf/3-Th-Ta, V/Ti/1,000 diagrams (Figures 8A,B) or the Th/Yb-Nb/Yb, TiO_2/Yb-Nb/Yb diagrams (Figures 8C,D).

The chemical compositions of the samples are consistent with Nb-enriched basalts in the TiO_2-Nb and Nb-Nb/U diagrams (Figure 9), with high Nb contents (9.02–15.68 ppm, mean 13.25 ppm), high Nb/U ratios (16.16–39.23) and mantle-standardised La/Nb ratios <2 (0.84–1.06). In general, Nb-enriched basalts are the direct product of oceanic plate subduction, formed by partial melting of mantle wedge peridotites accounted for by adakite melts (Sajona et al., 1993, 1996). La/Sm-La can be effectively used to differentiate between partial melting and fractional crystallization of magma (Allegre and Minster, 1978). La and Sm are not affected by mineral alteration from the magma sources, and Yb is compatible with garnet but not with spinel. Sm/Yb ratios are therefore effective in tracing source minerals, and La/Sm ratios can be valuable in limiting the composition of the sources (Aldanmaz, 2002; Green, 2006; Sun et al., 2017). In the La/Sm-La diagram, the data from this study are concentrated along the partial melting line (Figure 10A). In the Sm/Yb-La/Sm diagram, most of the points lie on the spinel lherzolite melting curve, except for two which fall on the garnet lherzolite zone (Figure 10A). This leads us to believe that the eclogites originated from the partial melting of lherzolite containing spinel and minor garnet, which may have been undergone metasomatism by subduction fluids or melt. It is comparable to the source of Nb-enriched eclogites in the Heihe area, western Yunnan (Wang W. et al., 2021).

Sr-Nd isotopes are well traced for the source region, but Sr is easily affected by seawater or hydrothermal fluids, relatively $^{143}Nd/^{144}Nd$ is less sensitive to metamorphism (Zindler and Hart., 1986). In this study, $\varepsilon_{Nd}(t)$ values are positive (mean 3.63, Table 1) and the $^{143}Nd/^{144}Nd$ ratios is similar to that of the enriched mantle, implicating it is the magma source of the protolith.

In high grade metamorphic rocks, metamorphism results in lower Lu/Hf ratios for metamorphic zircons due to a process in which the Lu content decreases and the Hf content increases (Chen et al., 2007). Such ratios are not available to source tracing of protoliths (Wu et al., 2007). For the study of protolith chemistry, the only suitable zircon Lu-Hf isotopic data are those with magmatic crystallization, and the magmatic crystallization ages are required for the calculation of initial Hf isotopic values (Zheng et al., 2007). For the Bangbing eclogites, there are no magma crystallized cores or mantles retained in the metamorphic zircons. Consequently, it is not possible to discuss their protolithic origin in terms of Hf isotopes. Thus, the initial Hf isotope ratios were calculated based on the magmatic protolith age obtained from the retrograde eclogites from the Mengku area in the CMSZ (Wang et al., 2019). The resulting $\varepsilon_{Hf}(t)$ values (mean 15.49) are more than three times larger than $\varepsilon_{Nd}(t)$, with a positive correlation between Nd and Hf isotopes. It is inferred that these values cannot characterize the Hf isotopic content of the source region.

As discussed above, based on the whole-rock geochemical signatures generally characteristic of tholeiites, rare earth and trace element patterns, and positive $\varepsilon_{Nd}(t)$, $\varepsilon_{Hf}(t)$ values, we infer that the original Nb-enriched basalts were produced by partial melting of the oceanic asthenospheric mantle similar to the E-MORB sources.

Implication for the tectonic evolution of the Paleo-Tethys

In the previous studies, the Changning-Menglian Ocean has begun to subduct at 473–471 Ma (Wang et al., 2013; Liu et al., 2017). The Middle Ordovician O-type adakitic high-magnesium tonalite in the Niujingshan area (Wang F. et al., 2016), the

451–456 Ma volcanism in the Huimin area (Nie et al., 2015; Xing et al., 2017), and the Early-Middle Ordovician magmatic arc occurring in the Lincang granitic batholith in the Bangbin area (Peng et al., 2018; Han et al., 2020) are all products of the eastward subduction of the Proto-Tethys Ocean. The Late Silurian (421–419 Ma) island-arc volcanic rocks in the Dazhonghe area (Mao et al., 2012) represent a continental margin magmatic arc formed by eastward subduction of the Proto-Tethys Ocean during the Late Paleozoic (Figure 11A).

With the end of the subduction of the Proto-Tethys Ocean, the development of the Paleo-Tethys Ocean has initiated. The latter succeeded and evolved on the basis of the same ocean basin of the former (Wang et al., 2018). The Paleo-Tethys Ocean extended and subducted concurrently during the Devonian and Early Carboniferous-Late Permian periods. Basic-ultrabasic magmatism associated with the extension of the ocean basin developed in the Tongchangjie and Niujingshan area (Wang et al., 2017). The extension of the ocean basin was coupled with the formation of deep-sea sedimentary rocks (oceanic islands-seamounts) during the Carboniferous to Permian (Pan et al., 2020). The Lincang-Menghai magmatic arc includes a series of magmatic events associated with subduction (Peng, et al., 2006; Kong, et al., 2012; Nie et al., 2016). All the above lithological records indicate the occurrence of eastward subduction of the Paleo-Tethys Ocean during this period (Figure 11B).

Large-scale subduction of the Paleo-Tethys Ocean occurred in the Early-Middle Triassic and lasted until the beginning of Late Triassic. The identified high-pressure metamorphic protoliths ages in the CMSZ range from 451 to 260 Ma (Zhao et al., 1994; Fan et al., 2015; Wang et al., 2019), with peak metamorphic ages of 246–233 Ma (Wang et al., 2019, 2021). In this study, we obtained a peak metamorphic age of 238 Ma for the eclogites in Bangbing area. The 13 Ma range in peak metamorphic ages suggests that continuous subduction was occurring in the Changning-Menglian Ocean during this period. With continuous subduction, part of OIB and MORB oceanic crusts were involved in subduction channels due to tectonic effects such as shovelling and scraping to depths of more than 100 km (Lisun et al., 2017). Concurrently, arc magmatism associated with subduction occurred in the Lincang-Menghai area to the east (254–239 Ma; Yu et al., 2003; Peng et al., 2006; Liu DL. et al., 2008; Hennig et al., 2009). Oceanic crust from various sources and different epochs migrated and accreted towards active continental margins (trenches) in response to the subduction (Figure 11C).

After the cessation of Late Triassic subduction, the Changning-Menglian Ocean closed and proceeded to the arc-continent and continent-continent collision orogeny. As a result of mantle upwelling leading to partial melting of crustal material, a massive Lincang granitic batholith and associated post-collisional volcanic rocks occurred on the eastern side of the suture zone (231–215 Ma; Nie et al., 2012; Kong et al., 2012; Zhao et al., 2018). The 220–229 Ma metamorphic ages obtained in our study may correspond to such magmatic events. The time between the peak metamorphism and exhumation of the UHP/HP metamorphic rocks was thus <31 Ma. This range indicates a rapid rate of uplift, possibly 3–6 mm/a (Li, et al., 2015), during a relatively short exhumation. The few eclogites and blueschist exhumed to the surface occurred as variable-sized lenses within Grt-Ph-Qz schists in accretionary complex (Figure 11D).

Conclusion

1. The geochemical composition of Bangbing eclogites is similar to tholeiitic basalts. The samples show E-MORB-like geochemical affinities, and exhibit isotopic $\varepsilon_{Nd}(t)$ values of 3.14–4.49 and $\varepsilon_{Hf}(t)$ of 14.64–16.41, respectively. The Nb-enriched mafic protoliths of these samples suggested to be derived from oceanic crust which were produced by partial melting of the enriched mantle sources.
2. The youngest group of detrital zircon ages peaking at 450–600 Ma in the metasedimentary rocks, in which the eclogites were hosted, constrain the maximum depositional age for the Lancang Group to the Early Paleozoic.
3. The magmatic zircon grains separated from the eclogites samples yield a wide range of U-Pb ages, which may be capture zircon ages rather than protolith crystallization. The metamorphic zircon grains yield a weighted mean age of 238 ± 2 Ma. This data represents the time when eclogite-facies metamorphism occurred according to CL images, zircon trace element analysis. Combined with previous age results in the CMSZ, we propose that continued subduction of the Paleo-Tethys oceanic crust occurred during the Early-Middle Triassic (246–233 Ma), and rapid exhumation in the Late Triassic (231–215 Ma).
4. The Bangbeng Nb-enriched eclogites are products of oceanic crustal subduction and occurred as lenses in Grt-Ph-Qz schists after a rapid evolution. Their presence indicates that the Changning-Menglian suture zone is a typical oceanic subduction-accretionary orogeny belt.

Data availability statement

The original contributions presented in the study are included in the article/supplementary material, further inquiries can be directed to the corresponding author.

Author contributions

YF: Conceptualization, Formal analysis, Investigation, Writing-Original Draft, Writing-Review and Editing. ZP: Formal analysis, Resources, Writing-Review and Editing, Supervision, Funding acquisition. GW: Conceptualization, Resources, Funding acquisition. JH: Conceptualization, Formal analysis, Investigation. ZZ: Conceptualization, Investigation. JG: Conceptualization, Investigation. FR: Conceptualization, Investigation.

Funding

This study was supported by the National Natural Science Foundation of China (No. 92055314, Tethyan tectonic maps compilation and regional comparative researches and No. 41602091), the China Geological Survey (No. DD20221635, Regional Basic Geological Survey of the Southwest China), and the China Scholarship Council (CSC, grant No. 202008515090).

Acknowledgments

We would like to express our sincere gratitude to Pan Guitang, Li Wenchang, Wang Liquan and Wang Baodi for their help in the field work, and to Chen Hongfang of the Wuhan Sample Solution Analytical Technology Company Co., Ltd. For her help in Zircon U-Pb dating. We would also appreciate the valuable comments from the reviewers.

Conflict of interest

The authors declare that the research was conducted in the absence of any commercial or financial relationships that could be construed as a potential conflict of interest.

Publisher's note

All claims expressed in this article are solely those of the authors and do not necessarily represent those of their affiliated organizations, or those of the publisher, the editors and the reviewers. Any product that may be evaluated in this article, or claim that may be made by its manufacturer, is not guaranteed or endorsed by the publisher.

References

Adanmaz, E. (2002). Mantle source characteristics of alkali basalts and basanites in an extensional intracontinental plate setting Western anatolia, Turkey: Implications for multi-stage melting. *Int. Geol. Rev.* 5 (44), 440–457. doi:10.2747/0020-6814.44.5.440

Allegre, C. J., and Minster, J. F. (1978). Quantitative models of trace element behavior in magmatic processes. *Earth Planet. Sci. Lett.* 38 (1), 1–25. doi:10.1016/0012-821x(78)90123-1

Bao, P. S., Xiao, X., Wang, J., Li, C., and Hu, K. (1999). Studies on the blueschist belt in the Shuanghu region, central northern Tibet and its tectonic implications. *Cont. Dyn.* 73 (4), 302–314. (in Chinese with English abstract). https://kns.cnki.net/kcms/detail/detail.aspx?FileName=DZXE199904001&DbName=CJFQ1999

Becker, H., Jochum, K. P., and Carlson, R. W. (1999). Constraints from High-Pressure veins in eclogites on the composition of hydrous fluids in subduction zones. *Chem. Geol.* 160 (4), 291–308. doi:10.1016/s0009-2541(99)00104-7

Blichert-Toft, J., and Albarède, F. (1997). The Lu-Hf isotope geochemistry of chondrites and the evolution of the mantle-crust system. *Earth Planet. Sci. Lett.* 148, 243–258. doi:10.1016/S0012-821X(97)00040-X

Chen, D. G., Ni, T., and Xie, L. W. (2007). Zircon Lu-Hf isotopic compositions of ultra-high pressure metamorphic rocks from Dabie Terrain, China. *Acta Petrol. Sin.* 23 (2), 331–342. doi:10.3969/j.issn.1000-0569.2007.02.013

Clarke, G. L., Powell, R., and Fitzherbert, J. A. (2006). The lawsonite paradox: A comparison of field evidence and mineral equilibria modelling. *J. Metamorph. Geol.* 24, 715–725. doi:10.1111/j.1525-1314.2006.00664.x

Condie, K. C. (1989). Geochemical changes in baslts and andesites across the Archean-Proterozoic boundary: Identification and significance. *Lithos* 23 (1-2), 1–18. doi:10.1016/0024-4937(89)90020-0

Deng, J., Wang, Q. F., Li, G. J., Li, C., and Wang, C. (2014). Tethys tectonic evolution and its bearing on the distribution of important mineral deposits in the Sanjiang region, SW China. *Gondwana Res.* 26 (2), 419–437. doi:10.1016/j.gr.2013.08.002

Dong, Y. S., and Li, C. (2009). Discovery of eclogite in the guoganjianian mountain, central Qiangtang area, northern tibet, China. *Geo-logical Bull. China* 28 (9), 1197–1200. (in Chinese with English abstract). doi:10.3969/j.issn.1671-2552.2009.09.006

Dong, Y. S., Li, C., Shi, J. R., Zhang, X. Z., and Wang, S. Y. (2010). Forming process of the high-pressure metamorphic belt in central Qiangtang, Tibet. *Acta Petrol. Sin.* 26 (7), 2099–2105. (in Chinese with English abstract).https://kns.cnki.net/kcms/detail/detail.aspx?FileName=YSXB201007012&DbName=CJFQ2010

Ernst, W. G. (2006). Preservation/exhumation of ultrahigh-pressure subduction complexes. *Lithos* 92, 321–335. doi:10.1016/j.lithos.2006.03.049

Fan, W. M., Wang, Y. J., Zhang, Y. H., Zhang, Y. Z., Jourdan, F., Zi, J. W., et al. (2015). Paleotethyan subduction process revealed fromTriassic blueschists in the Lancang tectonic belt of Southwest China. *Tectonophysics* 662, 95–108. doi:10.1016/j.tecto.2014.12.021

Ferry, J. M., and Watson, E. B. (2007). New thermodynamic models and revised calibrations for the Ti-in-zircon and Zr-in-rutile thermometers. *Contrib. Mineral. Pet.* 154, 429–437. doi:10.1007/s00410-007-0201-0)

Fu, Y. Z., Peng, Z. M., Wang, B. D., Wang, G. Z., Hu, J. F., Guan, J. L., et al. (2021). Petrology and metamorphism of glaucophane eclogites in changning-menglian suture zone, bangbing area, southeast Tibetan plateau: A evidence for paleo-tethyan subduction. *China Geol.* 4 (1), 111–116. doi:10.31035/cg2021017

Green, N. L. (2006). Influence of slab thermal structure on basalt source regions and melting conditions: REE and HFSE constraints from the garibaldi volcanic belt, northern cascadia subduction system. *Lithos* 87, 23–49. doi:10.1016/j.lithos.2005.05.003

Griffin, W. L., Pearson, N. J., Belousova, E., Jackson, S. E., Van, A. E., O'Reilly, S. R., et al. (2000). The Hf isotope composition of cratonic mantle: LAM-MC-ICP MS analysis of zircon megacrysts in kimberlites. *Geochimica Cosmochimica Acta* 64 (1), 133–147. doi:10.1016/S0016-7037(99)00343-9

Han, W. W., Peng, Z. M., Zhang, J., Guan, J. L., Hu, J. F., and Liu, Y. H. (2020). U-Pb dating of zircon, Hf isotope composition and tectonic significance of the albite-leptite of the Lancang Group in the Shuangjiang area of Western Yunnan, China. *Acta Geol. Sin.* 94 (4), 1282–1294. doi:10.19762/j.cnki.dizhixuebao.2020038

Hennig, D., Lehmann, B., Frei, D., Belyatsky, B., Zhao, X. F., Cabral, A. R., et al. (2009). Early permian sea floor to continental arc magmatism in the eastern paleo-tethys: U–Pb age and Nd–Sr isotope data from the southern lancangjiang zone, yunnan, China. *Lithos* 113 (3-4), 408–422. doi:10.1016/j.lithos.2009.04.031

Hofmnn, A. W. (1988). Chemical differentiation of the Earth: The relationship between mantle, continental crust, and Oceanic crust. *Earth Planet. Sci. Lett.* 90 (3), 297–314. doi:10.1016/0012-821x(88)90132-x

Hou, Z. Q., Mo, X. X., Zhu, Q. W., and Shen, S. Y. (1996). Mantle plume in the Sanjiang paleo-tethyan lithosphere: Evidence from mid-ocean ridge basalts. *Acta Geosci. Sin.* 17 (4), 362–375. https://kns.cnki.net/kcms/detail/detail.aspx?FileName=DQXB604.002&DbName=CJFQ1996.

Hu, Z. C., Liu, Y. S., Gao, S., Liu, W. G., Yang, L., Zhang, W., et al. (2012). Improved *in situ* Hf isotope ratio analysis of zircon using newly designed X skimmer cone and jet sample cone in combination with the addition of nitrogen by laser ablation multiple collector ICP-MS. *J. Anal. At. Spectrom.* 27, 1391–1399. doi:10.1039/c2ja30078h

Kepezhinskas, P., Defant, M. J., and Drummond, M. S. (1996). Progressive enrichment of island arc mantle by melt-peridotite interaction inferred from Kamchatka xenoliths. *Geochim. Cosmochim. Acta* 60 (7), 1217–1229. doi:10.1016/0016-7037(96)00001-4

Kong, H. L., Dong, G. C., Mo, X. X., Zhao, Z. D., Zhu, D. C., Wang, S., et al. (2012). Petrogenesis of Lincang granites in Sanjiang area of Western Yunnan Province: Constraints from geochemistry, zircon U-Pb geochronology and Hf isotope. *Acta Petrol. Sin.* 28, 1438–1452. https://kns.cnki.net/kcms/detail/detail.aspx?FileName=YSXB201205010&DbName=CJFQ2012

Li, C., Dong, Y. S., Zhai, Q. G., Yu, J. J., and Huang, X. P. (2008). High-pressure metamorphic belt in Qiangtang, Qinghai-Tibet Plateau, and its tectonic significance. *Geol. Bull. China* 27 (1), 27–35. (in Chinese with English abstract). doi:10.3969/j.issn.1671-2552.2008.01.003

Li, C., Zhai, Q. G., Chen, W., Yu, J. J., Huang, X. P., and Zhang, Y. (2006). Ar-Ar chronometry of the eclogite from central Qiangtang area, Qinghai-Tibet Plateau. *Acta Petrol. Sin.* 22 (12), 2843–2849. doi:10.3969/j.issn.1000-0569.2006.12.003

Li, C., Zhai, Q. G., Dong, Y. S., Liu, S., Xie, C. M., and Wu, Y. W. (2009). High-pressureeclogite-blueschist metamorphic belt and closure of Paleo-Tethys ocean in central Qiangtang, qinghai-tibet plateau. *J. Earth Sci.* 20, 209–218. doi:10.1007/s12583-009-0021-4

Li, C. F., Li, X. H., Li, Q. L., Guo, J. H., and Yang, Y. H. (2012). Rapid and precise determination of Sr and Nd isotopic ratios in geological samples from the same filament loading by thermal ionization mass spectrometry employing a single-step separation scheme. *Anal. Chim. Acta* 727, 54–60. doi:10.1016/j.aca.2012.03.040

Li, J., Sun, Z. B., Xu, G. X., Zhou, K., Huang, L., Tian, S. M., et al. (2015). Firstly discovered garnet-amphibolite from Mengku area, Shuangjiang county, western yunnan province, China. *Acta Mineral. Sin.* 35, 421–424. doi:10.16461/j.cnki.1000-4734.2015.04.001

Li, J., Sun, Z. B., Huang, L., Xu, G. X., Tian, S. M., Deng, R. H., et al. (2017). P-T-t path and geological significance of retrograded eclogites from Mengku area in Western Yunnnan Province, China. *Acta Petrol. Sin.* 33, 2285–2301. https://kns.cnki.net/kcms/detail/detail.aspx?FileName=YSXB201707022&DbName=CJFQ2017

Li, Q. L., Li, S. G., Hou, Z. H., Hong, J. A., and Yang, W. (2004). High-pressure metamorphic neozoic zircon SHRIMP-U-Pb dating, trace elements and mineral inclusions in the Qinglongshan eclogites. *Sci. Bull.* 49 (22), 2329–2334. https://kns.cnki.net/kcms/detail/detail.aspx?FileName=KXTB20042200D&DbName=CJFQ2004.

Liang, X., Wang, G. H., Yang, B., Ran, H., Zheng, Y., Du, J., et al. (2017). Stepwise exhumation of the Triassic Lanling high-pressure metamorphic belt in Central Qiangtang, Tibet: Insights from a coupled study of metamorphism, deformation, and geochronology. *Tectonics* 36, 652–670. doi:10.1002/2016tc004455

Liu, D. L., Liu, J. S., Zhang, C. H., and Zhou, Y. G. (2008a). Geological characteristics and tectonic setting of Yunxian granite in the northern part of South Lancangjiang convergent margin, Western Yunnan Province. *Acta Petrologica Mineralogica* 27 (1), 23–31. doi:10.3969/j.issn.1000-6524.2008.01.003

Liu, G. C., Sun, Z. B., Zeng, W. T., Feng, Q. L., Huang, L., and Zhang, H. (2017). The age of Wanhe ophiolitic mélange from Mengku area, Shuangjiang County, Western Yunnan Province, and its geological significance. *Acta Petrologica Mineralogica* 36, 163–174. doi:10.3969/j.issn.1000-6524.2017.02.003

Liu, Y., Santosh, M., Zhao, Z. B., Niu, W. C., and Wang, G. H. (2011). Evidence for palaeo-Tethyan oceanic subduction within central Qiangtang, northern Tibet. *Lithos* 127, 39–53. doi:10.1016/j.lithos.2011.07.023

Liu, Y. S., Gao, S., Hu, Z. C., Gao, C. G., Zong, K. Q., and Wang, D. B. (2010). Continental and oceanic crust recycling-induced melt-peridotite interactions in the trans-north China orogen: U-Pb dating, Hf isotopes and trace elements in zircons from mantle xenoliths. *J. Petrology* 51 (1-2), 537–571. doi:10.1093/petrology/egp082

Liu, Y. S., Hu, Z. C., Gao, S., Gunther, D., Xu, J., Gao, C. G., et al. (2008b). *In situ* analysis of major and trace elements of anhydrous minerals by LA-ICP-MS without applying an internal standard. *Chem. Geol.* 257 (1-2), 34–43. doi:10.1016/j.chemgeo.2008.08.004

Ludwig, K. R. (2003). *User's manual for Isoplot 3.0: A geochronological tool kit for microsoft Excel*. California. Berkeley Geochronology Center Special Publication, 41–70.

Mao, X. C., Wang, L. Q., Li, B., Wang, B. D., Wang, D. B., Yin, F. G., et al. (2012). Discovery of the Late Silurian volcanic rocks in the Dazhonghe area, Yunxian-Jinggu volcanic arc belt, Western Yunnan, China and its geological significance. *Acta Petrol. Sin.* 28 (5), 1517–1528. (in Chinese with English abstract). https://kns.cnki.net/kcms/detail/detail.aspx?FileName=YSXB201205016&DbName=CJFQ2012

Martin, H., Smithies, R. H., Rapp, R., Moyen, J. F., and Champion, D. (2005). An overview of adakite, tonalite–trondhjemite–granodiorite (TTG), and sanukitoid: Relationships and some implications for crustal evolution. *Lithos* 79 (1-2), 1–24. doi:10.1016/j.lithos.2004.04.048

Maruyama, S., Lou, J. G., and Tarabayashi, M. (1996). Blueschists and eclogites of the world and their exhumation. *Int. Geol. Rev.* 38, 485–594. doi:10.1080/00206819709465347

Metcalfe, I. (2013). Gondwana dispersion and Asian accretion: Tectonic and palaeogeographic evolution of eastern Tethys. *J. Asian Earth Sci.* 66, 1–33. doi:10.1016/j.jseaes.2012.12.020

Nie, F., Dong, G. C., Mo, X. X., Zhu, D. C., Dong, M. L., and Wang, X. (2012). Geochemistry, zircon U-Pb chronology of the Triassic granites in the Changning-Menglian suture zone and their implications. *Acta Petrol. Sin.* 28 (5), 1465–1476. (in Chinese with English abstract). https://kns.cnki.net/kcms/detail/detail.aspx?FileName=YSXB201205012&DbName=CJFQ2012"

Nie, X. M., Feng, Q. L., Metcalfe, I., Baxter, A. T., and Liu, G. C. (2016). Discovery of a late devonian magmatic arc in the southern lancangjiang zone, western yunnan: Geochemical and ZirconU-Pb geochronological constraints on the evolution of tethyan ocean basins in SW China. *J. Asian Earth Sci.* 118, 32–50. doi:10.1016/j.jseaes.2015.12.026

Nie, X. M., Feng, Q. L., Qian, X., and Wang, Y. J. (2015). Magmatic record of Prototethyan evolution in SW Yunnan, China: Geochemical, zircon U–Pb geochronological and Lu–Hf isotopic evidence from the Huimin metavolcanic rocks in the southern Lancangjiang zone. *Gondwana Res.* 28, 757–768. doi:10.1016/j.gr.2014.05.011

Pan, G. T., Chen, Z. L., Li, X. Z., and Yan, Y. J. (1997). *Geological tectonic formation and evolution of the Eastern Tethys*. Beijing: Geological Press, 1–128. (in Chinese).

Pan, G. T., Wang, L. Q., Geng, Q. R., Yin, F. G., Wang, B. D., Wang, D. B., et al. (2020). Space-time structure of the bangonghu-shuanghu-nujiang-changning-menglian mega-suture zone: A discussion on geology and evolution of the Tethys ocean. *Sediment. Geol. Tethyan Geol.* 40 (3), 1–19. doi:10.19826/j.cnki.1009-3850.2020.07001

Pan, G. T., Wang, L. Q., and Zhu, D. C. (2004). Thoughts on some important scientific problems in regional geological survey of the Qinghai-Tibet Plateau. *Geol. Bull. China* 23 (1), 12–19. doi:10.3969/j.issn.1671-2552.2004.01.007

Pearce, J. A. (2008). Geochemical fingerprinting of oceanic basalts with applications to ophiolite classification and the search for Archean oceanic crust. *Lithos* 100 (1-4), 14–48. doi:10.1016/j.lithos.2007.06.016

Peng, T. P., Wang, Y. J., Fan, W. M., Liu, D., and Miao, L. (2006). SHRIMP zircon U-Pb geochronology of early Mesozoic felsic igneous rocks from the southern Lancangjiang and its tectonic implications. *Sci. China (Series D)* 36, 123–132. doi:10.3969/j.issn.1674-7240.2006.02.002

Peng, X. J., and Luo, W. L. (1982). The discovery and earth tectonic significance of the blueschist belt in lancangjiang south segment of west yunnan. *Regional Geol. China* 2, 69–75. https://kns.cnki.net/kcms/detail/detail.aspx?FileName=ZQYD198202007&DbName=CJFQ1982

Peng, Z. M., Fu, Y. Z., Wang, G. Z., Guan, J. L., Geng, Q. R., Hu, J. F., et al. (2020a). The results of geoehronological, geochemical and Sr-Nd-Hf isotopic investigations on amphibolites in the Qingping Region, Changning-Menglian Suture Zone. *Acta Geol. Sin.* 94 (2), 511–526. doi:10.19762/j.cnki.dizhixuebao.2019113

Peng, Z. M., Wang, B. D., Hu, J. F., Fu, Y. Z., Wang, G. Z., and Zhang, J. (2020b). Determination and significance of Early Palacozoic accretionary complexes in the Western Yunnnan Province一New cognition based on the geological survey of Wendong Sheet (1:50000). *Geol. China* 0, 1–21. https://kns.cnki.net/kcms/detail/detail.aspx?FileName=DIZI20200407001&DbName=CAPJ2020

Peng, Z. M., Wang, G. Z., Wang, B. D., Wang, L. Q., Fu, Y. Z., Guan, J. L., et al. (2019). Discovery of glaucophane eclogites within the Lancang group in bangbing area, Western yunnan. *J. Chengdu Univ. Technol. (Science& Technol. Ed.* 46 (5), 639–640. (in Chinese with English abstract). doi:10.3969/j.issn.1671-9727.2019.05.14

Peng, Z. M., Zhang, J., Guan, J. L., Zhang, Z., Han, W. W., and Fu, Y. Z. (2018). The discovery of early-middle Ordovician granitic gneiss from the giant Lincang batholith in Sanjiang area of Western Yunnan and its geological implications. *Earth Sci.* 43, 2571–2585. (in Chinese with English abstract). doi:10.3799/dqkx.2018.102

Rubatto, D. (2002). Zircon trace element geochemistry: Partitioning with garnet and the link between U-Pb ages and metamorphism. *Chem. Geol.* 184, 123–138. doi:10.1016/s0009-2541(01)00355-2

Rudnick, R., Barth, M., Horn, I., and McDonough, W. F. (2000). Rutile-bearing refractory eclogites: Missing link between continents and depleted mantle. *Science* 287, 278–281. doi:10.1126/science.287.5451.278

Sajona, F. G., Maury, R. C., Bellon, H., Cotton, J., and Defant, M. J. (1996). High field strength element enrichment of pliocene—pleistocene island arc basalts, zamboanga peninsula, western mindanao (Philippines). *J. Petrol.* 3 (37), 693–726. doi:10.1093/petrology/37.3.693

Sajona, F. G., Maury, R. C., Bellon, H., Cotton, J., Defant, M. J., and Pubellier, M. (1993). Initiation of subduction and the generation of slab melts in Western and eastern Mindanao, Philippines. *Geology* 21 (11), 1007–1010. doi:10.1130/0091-7613(1993)021<1007:IOSATG>2.3.CO;2

Shervais, J. W. (1982). Ti-V plots and the petrogenesis of modern and ophiolitic lavas. *Earth Planet. Sci. Lett.* 59, 101–118. doi:10.1016/0012-821x(82)90120-0

Söderlund, U., Patchett, P. J., Vervoot, J. D., and Isachsen, C. E. (2004). The ^{176}Lu decay constant determined by Lu-Hf and U-Pb isotope systematics of Precambrian mafic intrusions. *Earth Planet. Sci. Lett.* 219, 311–324. doi:10.1016/S0012-821X(04)00012-3

Sun, S. S., and McDonough, W. F. (1989). Chemical and isotopic systematics of oceanic basalts: Implications for mantle composition and processes. *Geol. Soc. Lond. Spec. Publ.* 42, 313–345. doi:10.1144/gsl.sp.1989.042.01.19

Sun, W. D., Williams, I., and Li, S. G. (2002). Carboniferous and triassic eclogites in the Western dabie mountains, east-central China: Evidence for protracted convergence of the north and south China blocks. *J. Metamorph. Geol.* 20, 873–886. doi:10.1046/j.1525-1314.2002.00418.x

Sun, Z. B., Hu, S. B., Zhou, K., Zhou, T. Q., Zhao, J. T., Wang, Y. X., et al. (2019). Petrology, mineralogy and metamorphic P-T path of eclogites from the Qianmai area, Lancang County, Western Yunnan Province. *Geol. Bull. China* 38 (7), 1105–1115. (in Chinese with English abstract). https://kns.cnki.net/kcms/detail/detail.aspx?FileName=ZQYD201907004&DbName=CJFQ2019

Sun, Z. B., Li, J., Zhou, K., Zeng, W. T., Duan, X. D., Zhao, J. T., et al. (2017). Lithogeochemistry characteristics and geological significance of retrograde eclogite in Mengku area, Shuangjiang County, Western Yunnan Province, China. *Geoscience* 31, 746–756. (in Chinese with English abstract). doi:10.3969/j.issn.1000-8527.2017.04.009

Sun, Z. B., Li, J., Zhou, K., Zeng, W. T., Wu, J. L., Hu, S. B., et al. (2018). Zircon U-Pb age and geological significance of retro-graded eclogites from Mengku area in Western Yunnan Province. *Geol. Bull. China* 37 (11), 2032–2043. (in Chinese with English abstract). doi:10.12097/j.issn.1671-2552.2018.11.009

Wang, B. D., Wang, L. Q., Pan, G. T., Yin, F. G., Wang, D. B., and Tang, Y. (2013). U-Pb zircon dating of Early Paleozoic gabbro from the Nantinghe ophiolite in the Changning-Menglian suture zone and its geological implication. *Chin. Sci. Bull.* 58, 920–930. doi:10.1007/s11434-012-5481-8

Wang, B. D., Wang, L. Q., Wang, D. B., Yin, F. G., He, J., Peng, Z. M., et al. (2018). Tectonic evolution of the changning-menglian proto-paleo Tethys ocean in the Sanjiang area, southwestern China. *Earth Sci.* 43 (8), 2527–2550. (in Chinese with English abstract). https://kns.cnki.net/kcms/detail/detail.aspx?FileName=DQKX201808001&DbName=CJFQ2018

Wang, D. B., Luo, L., Tang, Y., Yin, F. G., Wang, B. D., and Wang, L. Q. (2016a). Zircon U-Pb dating and petrogenesis of Early Paleozoic adakites from the Niujingshan ophiolitic mélange in the Changning-Menglian suture zone and its geological implications. *Acta Petrol. Sin.* 32, 2317–2329. (in Chinese with English abstract). https://kns.cnki.net/kcms/detail/detail.aspx?FileName=YSXB201608006&DbName=CJFQ2016

Wang, F., Liu, F. L., Ji, L., and Liu, L. S. (2017). LA-ICP-MS U-Pb dating of detrital zircon from low-grade metamorphic rocks of the Lancang Group in the Lancangjiang Complex and its tectonic implications. *Acta Petrol. Sin.* 33, 2975–2985. (in Chinese with English abstract). https://kns.cnki.net/kcms/detail/detail.aspx?FileName=YSXB201709020&DbName=CJFQ2017

Wang, F., Liu, F. L., Ji, L., Liu, P. H., Cai, J., Tian, Z. H., et al. (2016b). Petrogenesis and metamorphic evolution of blueschist from Xiaoheijiang-Shangyun area in Lancangjiang metamorphic complex. *Acta Petrologica Mineralogica* 35, 804–820. (in Chinese with English abstract). doi:10.3969/j.issn.1000-6524.2016.05.005

Wang, H. N., Liu, F. L., Li, J., Sun, Z. B., Ji, L., Tian, Z. H., et al. (2019). Petrology, geochemistry and P-T-t path of lawsonite-bearing retrograded eclogites in the Changning-Menglian orogenic belt, southeast Tibetan Plateau. *J. Metamorph. Geol.* 39, 439–478. doi:10.1111/jmg.12462

Wang, H. N., Liu, F. L., Santosh, M., Cai, J., Wang, F., and Ji, L. (2020a). Rapid cold slab subduction of the Paleo-Tethys: Insights from lawsonite-bearing blueschist in the Changning-Menglian orogenic belt, southeastern Tibetan Plateau. *Gondwana Res.* 85, 189–223. doi:10.1016/j.gy.2020.01.001

Wang, H. N., Liu, F. L., Sun, Z. B., Ji, L., Cai, J., and Zhu, J. J. (2021a). Identification of continental-type eclogites in the Paleo-Tethyan Changning–Menglian orogenic belt, southeastern Tibetan Plateau: Implications for the transition from oceanic to continental subduction. *Lithos* 396-397, 106215–215. doi:10.1016/j.lithos.2021.106215

Wang, H. N., Liu, F. L., Sun, Z. B., Ji, L., Zh, J. J., Cai, J., et al. (2020b). A new HP–UHP eclogite belt identified in the southeastern Tibetan plateau: Tracing the extension of the main palaeo-tethys suture zone. *J. Petrology* 61, 1–45. doi:10.1093/petrology/egaa073

Wang, W., Zhang, X. P., Sun, Z. B., Tian, Y. G., Zhou, K., Li, X. J., et al. (2021b). Petrology and geochemistry of the eclogite in Heihe area of Lancang county, Western yunnan: The magmatism of the initial subduction of the oceanic crust. *Geol. Bull. China* 40 (7), 1057–1067. (in Chinese with English abstract). https://kns.cnki.net/kcms/detail/detail.aspx?FileName=ZQYD202107005&DbName=CJFQ2021

Wei, C. J., and Clarke, G. L. (2011). Calculated phase equilibria for MORB compositions: A reappraisal of the metamorphic evolution of lawsonite eclogite. *J. Metamorph. Geol.* 29, 939–952. doi:10.1111/j.1525-1314.2011.00948.x

Whitney, D. L., and Evans, B. W. (2010). Abbreviations for names of rock-forming minerals. *Am. Mineral.* 95, 185–187. doi:10.2138/am.2010.3371

Wood, D. A. (1980). The application of a ThHfTa diagram to problems of tectonomagmatic classification and to establishing the nature of crustal contamination of basaltic lavas of the British Tertiary Volcanic Province. *Earth Planet. Sci. Lett.* 1 (50), 11–30. doi:10.1016/0012-821X(80)90116-8

Wu, F. Y., Li, X. H., Zheng, Y. F., and Gao, S. (2007). Lu-Hf isotopic systematics and their applications in petrology. *Acta Petrol. Sin.* 23 (2), 185–220. (in Chinese with English abstract). doi:10.3321/j.issn:1000-0569.2007.02.001

Wu, Y. B., and Zheng, Y. F. (2004). Mineralogical studies on the Genesis of zircon and its constraints on the interpretation of U-Pb ages. *Sci. Bull.* 49 (16), 1589–1604. (in Chinese with English abstract). doi:10.3321/j.issn:0023-074X.2004.16.002

Xing, X., Wang, Y., Cawood, P. A., and Zhang, Y. (2017). Early paleozoic accretionary orogenesis along northern margin of gondwana constrained by high-Mg metaigneous rocks, SW Yunnan. *Int. J. Earth Sci.* 106, 1469–1486. doi:10.1007/s00531-015-1282-z

Xu, Y., wang, Q., Tang, G., Wang, J., Li, H., Zhou, J., et al. (2020). The origin of arc basalts: New advances and remaining questions. *Sci. China Earth Sci.* 50 (12), 1969–1991. doi:10.1007/s11430-020-9675-y

Yu, S. Y., Li, K. Q., Shi, Y. P., and Zhang, H. H. (2003). A study on the granodiorite in the middle part of lincang granite batholith. *Yunnan Geol.* 22 (4), 426–442. (in Chinese with English abstract). doi:10.3969/j.issn.1004-1885.2003.04.009

Zhai, M. G., Cong, B. L., and Zhang, R. Y. (1990). Distinguishing of two volcanic rock series in the Lancang Group, Yunnan Province, SW China and its geological implication. *Sci. China* 33, 968–979. (in Chinese with English abstract). https://kns.cnki.net/kcms/detail/detail.aspx?FileName=JBXG199008009&DbName=CJFQ1990

Zhai, Q. G., Jahn, B. M., Li, X. H., Zhang, R. Y., Li, Q. L., et al. (2017). Zircon U–Pb dating of eclogite from the Qiangtang terrane, north-central tibet: A case of metamorphic zircon with magmatic geochemical features. *Int. J. Earth Sci.* 106, 1239–1255. doi:10.1007/s00531-016-1418-9

Zhai, Q. G., Wang, J., and Wang, Y. (2009). Discovery of eclogite at gangmacuo area from gerze county, tibet, China. *Geol. Bull. China* 28 (12), 1720–1724. (in Chinese with English abstract). doi:10.3969/j.issn.1671-2552.2009.12.005

Zhai, Q. G., Zhang, R. Y., Jahn, B. M., Cai, L., Song, S. G., and Wang, J. (2011). Triassic eclogites from central Qiangtang, northern Tibet, China: Petrology, geochronology and metamorphic P–T path. *Lithos* 125, 173–189. doi:10.1016/j.lithos.2011.02.004

Zhang, L. F., Lü, Z., Zhang, G. B., and Song, S. G. (2008). The geological characteristics of oceanic-type UHP metamorphic belts and their tectonic implications: Case studies from Southwest Tianshan and North Qaidam in NW China. *Sci. Bull. (Beijing).* 53, 3120–3130. doi:10.1007/s11434-008-0386-2

Zhang, R. Y., Cong, B. L., and Han, X. L. (1990). Amphiboles of blueschist in west Yunnan region. *Sci. Geol. Sin.* 1, 43–53. (in Chinese with English abstract). https://kns.cnki.net/kcms/detail/detail.aspx?FileName=DZKX199001004&DbName=CJFQ1990

Zhang, X. Z., Dong, Y. S., Li, C., Shi, J. R., and Wang, S. Y. (2010). Geochemistry and tectonic significance of eclogites in central Qiangtang, Tibetan Plateau. *Geol. Bull. China* 29 (12), 1804–1814. (in Chinese with English abstract). doi:10.3969/j.issn.1671-2552.2010.12.008

Zhang, X. Z., Dong, Y. S., Li, C., Xie, C. M., Wang, M., Deng, M. R., et al. (2014). A record of complex histories from oceanic lithosphere subduction to continental subduction and collision: Constraints on geochemistry of eclogite and blueschist in Central Qiangtang, Tibetan Plateau. *Acta Petrol. Sin.* 30 (10), 2821–2834. (in Chinese with English abstract). https://kns.cnki.net/kcms/detail/detail.aspx?FileName=YSXB201410003&DbName=CJFQ2014

Zhang, Z. B., Li, J., Lü, G. X., Yu, H., and Wang, F. Z. (2004). Characteristics of blueschist in Shuangjiang tectonic mélange zone, West Yunnan province. *J. China Univ. Geosciences* 15 (2), 224–231. https://kns.cnki.net/kcms/detail/detail.aspx?FileName=ZDDY200402014&DbName=CJFQ2004

Zhao, F., Li, G. J., Zhang, P. F., Wang, C. B., Sun, Z. B., and Tang, X. (2018). Petrogenesis and tectonic implications of the Lincang batholith in the Sanjiang, Southwest China: Constraints by geochemistry, zircon U-Pb chronology and Hf isotope. *Acla Petrol. Sin.* 34 (5), 1397–1412. (in Chinese with English abstract). https://kns.cnki.net/kcms/detail/detail.aspx?FileName=YSXB201805013&DbName=CJFQ2018

Zhao, F., Xue, S. C., Li, G. J., Sun, Z. B., Tang, X., Hu, X. W., et al. (2021). Petrology and geochemistry of retrograde eclogites in the Changning-Menglian suture zone, southwest China: Insights into the Palaeo-Tethyan subduction and rutile mineralization. *Ore Geol. Rev.* 139, 104493. doi:10.1016/j.oregeorev.2021.104493

Zhao, J. (1993). A study of muscovites from the Lancang metamorphic belt in Western Yunnan and its geological significance. *Acta Petrologica Mineralogica* 12, 251–260. (in Chinese with English abstract). https://kns.cnki.net/kcms/detail/detail.aspx?FileName=YSKW199303006&DbName=CJFQ1993

Zhao, J., Zhong, D. L., and Wang, Y. (1994). Metamorphism of Lancang metamorphic belt, the Western Yunnan and its relation to deformation. *Acta Petrol. Sin.* 10, 27–40. (in Chinese with English abstract). doi:10.3321/j.issn:1000-0569.1994.01.003

Zheng, Y. F., Chen, R. X., Zhang, S. B., Tang, J., Zhao, Z. F., and Wu, Y. B. (2007). Zircon Lu-Hf isotope study of ultrahigh-pressure eclogite and granitic gneiss in the Dabie orogen. *Acta Petrol. Sin.* 23 (2), 317–330. (in Chinese with English abstract). doi:10.3321/j.issn:1000-0569.2007.02.012

Zheng, Y. F. (2012). Metamorphic chemical geodynamics in continental subduction zones. *Chem. Geol.* 328, 5–48. doi:10.1016/j.chemgeo.2012.02.005

Zhong, D. L. (1998). *The paleotethys orogenic belt in west of sichuan and yunnan*. Beijing: Science Publishing House China, 1–216. (in Chinese).

Zindler, A., and Hart, S. R. (1986). Chemical geodynamics. *Annu. Rev. Earth Planet. Sci.* 14, 493–571. doi:10.1146/annurev.ea.14.050186.002425